THE ASTROPHYSICAL JOURNAL SUPPLEMENT SERIES, 94:583–614, 1994 October

THE EMSS CATALOG OF X-RAY–SELECTED CLUSTERS OF GALAXIES. I. AN ATLAS OF CCD IMAGES OF 41 DISTANT CLUSTERS

I. M. GIOIA[1,2] AND G. A. LUPPINO
Institute for Astronomy, University of Hawaii, 2680 Woodlawn Drive, Honolulu, HI 96822. Internet: gioia@ifa.hawaii.edu, ger@ifa.hawaii.edu
Received 1993 December 6; accepted 1994 February 15

ABSTRACT

An atlas of deep, wide-field R-band CCD images of a complete sample of distant, X-ray-selected clusters of galaxies is presented. These clusters are the 41 most distant ($z \geq 0.15$) and most X-ray–luminous ($L_x \geq 2 \times 10^{44}$ ergs s^{-1}) clusters in the *Einstein Observatory* Extended Medium Sensitivity Survey (EMSS) catalog that are observable from Mauna Kea ($\delta > -40°$). The sample spans a redshift range of $0.15 \leq z \leq 0.81$ and includes at least two and possibly as many as six rich clusters with $z > 0.5$. For the most part, the data are of superior quality, with a median seeing of 0\".8 FWHM and coverage of at least 1 Mpc × 1 Mpc in the cluster frame ($H_0 = 50$; $q_0 = 1/2$).

In addition, we update the available optical, X-ray, and radio data on the entire EMSS sample of 104 clusters. We outline the cluster selection criteria in detail and emphasize that X-ray-selected cluster samples may prove to be more useful for cosmological studies than optically selected samples. The EMSS cluster sample in particular can be exploited for diverse cosmological investigations, as demonstrated by the detection of evolution in the X-ray luminosity function previously reported, and more recently by the discovery of a large number of gravitationally lensed images in these clusters.

Subject headings: atlases — galaxies: clustering — gravitational lensing — X-rays: galaxies

1. INTRODUCTION

Distant clusters of galaxies provide information about the early universe. They can be used for cosmological tests such as those based on the magnitude-redshift relation or the Sunyaev-Zel'dovich effect. They can be used as markers of large-scale structure. Changes in their properties as a function of look-back time are a record of cosmic evolution. In the past, cluster samples have been selected from optical surveys such as those of Abell (1958), Abell, Corwin, & Olowin (1989), Gunn, Hoessel, & Oke (1986), or Couch et al. (1991). However, optical selection involves the detection of a surface density enhancement of galaxies against a rich and variable background, which sometimes leads to false identifications due to superposition effects (see Frenk et al. 1990), especially at high redshifts.

Superposition effects can be avoided if clusters are selected based on the X-ray emission from the intracluster gas, rather than on the number density of optical galaxies. Clusters of galaxies are known to be very luminous X-ray sources, with the X-ray luminosities often exceeding 3×10^{43} ergs s^{-1}. Projection effects are much less severe in the X-ray than in the visible. First, no cluster will be lost due to superposition onto a smaller than average background because the surface brightness of the central cluster X-ray emission is several hundred times that of the X-ray background. Second, few clusters will be found which are actually the superposition of less rich systems because the X-ray luminosity of a cluster scales approximately as the cube of the richness (Bahcall 1977). Moreover, the X-ray temperature, which is analogous to the galaxy velocity dispersion, will be unaffected by projection. X-ray surveys and source detection methods are automated so that selection effects are well defined and quantifiable.

In 1992, we began an observational program to obtain deep, wide-field B and R CCD images of the most X-ray luminous, distant clusters selected from the *Einstein Observatory* Extended Medium Sensitivity Survey (EMSS) catalog (Gioia et al. 1990a; Stocke et al. 1991). Until the *ROSAT* North Ecliptic Pole region of the all-sky survey is completely identified, the EMSS is the only large (835 sources) and sensitive ($F_x \geq 7 \times 10^{-14}$ ergs cm^{-2} s^{-1} in the 0.3–3.5 keV band) X-ray survey from which a sample of distant clusters can be extracted. The goals of our survey were twofold. Our primary motivation was to search for gravitationally lensed arcs in a sample of X-ray–selected clusters. We also intended to compile a catalog of optical data on a complete sample of rich distant clusters that were not selected by traditional optical methods. The first results from the arc survey have already appeared in the literature (Luppino & Gioia 1992; Luppino et al. 1993; Le Fèvre et al. 1994) or are in preparation (Luppino et al. 1994). Here we present for the first time the deep CCD images acquired by us for the 41 clusters that constitute the arc survey sample. Subsequent papers will investigate the optical properties of the clusters that will be derived from the analysis of the arc survey data.

In § 2 we present and discuss the entire EMSS sample of 104 clusters from which the 41 cluster arc survey sample is extracted. Drawing upon new *ROSAT* data and additional imaging and spectroscopic data, we have updated the EMSS cluster list of 104 clusters (Gioia et al. 1990a; Stocke et al. 1991; Henry et al. 1992). In this section, we also update the status of the remaining EMSS unidentified fields that might possibly

[1] On leave from Istituto di Radioastronomia del CNR, Via Gobetti 101, I-40129, Bologna, Italy.
[2] Also Harvard-Smithsonian Center for Astrophysics, 60 Garden Street, Cambridge, MA 02138.

enhance the cluster sample. Our optical observations of the 41 most luminous and distant EMSS clusters, and a description of the data reduction are given in § 3. In § 4 we discuss qualitative properties of our X-ray–selected sample. Quantitative properties will be evaluated in subsequent papers in this series. Throughout, $H_0 = 50$ km s^{-1} Mpc^{-1} and $q_0 = \frac{1}{2}$ are assumed.

2. THE SAMPLE

2.1. *The EMSS Galaxy Cluster Sample*

The 41 clusters whose images appear in this atlas are extracted from the EMSS. Briefly, the EMSS is a flux-limited and homogeneous sample containing 835 sources discovered serendipitously in *Einstein* IPC images at high Galactic latitude. The limiting sensitivities of the IPC fields range from 5×10^{-14} to 3×10^{-12} ergs cm^{-2} s^{-1} in the 0.3–3.5 keV band. Details of the X-ray survey can be found in Gioia et al. (1990a). The optical identifications have been discussed in Stocke et al. (1991). Only 25 sources are still optically unidentified. It is thus possible to extract samples of X-ray–selected objects exclusively defined by their X-ray properties and suitable for statistical studies. There is a total of 104 clusters of galaxies in the EMSS. This count is corrected in line with recently acquired information on five so-called cooling flow galaxies. This term was adopted by Stocke et al. (1991) to indicate objects with low-ionization, optical emission-line spectra very similar to those of central galaxies in cooling flow clusters, but with no surrounding rich cluster present. Additional optical data and new *ROSAT* HRI pointed observations have helped us to clarify the nature of these sources. Three of them are now tentatively classified as clusters due to the presence of galaxies around them (MS 1125.3+4324, MS 1209.0+3917, and MS 1317.0−2111). The remaining two, MS 1826.5+7256 and MS 1019.0+5139, are identified with a flaring M star and a peculiar type of AGN or a possible BL Lac object, respectively (J. T. Stocke, private communication) and will be described elsewhere.

When selecting in X-rays there are a number of effects in the data that must be corrected. These effects include absorption by the Milky Way, the different sky coverage for different flux limits, correction for lost flux due to the finite 2′.4 × 2′.4 detection cell, and any variation of these effects with the different redshifts of the sources. We describe each of these corrections in turn. We recall here that the EMSS uses the so-called M-DETECT algorithm to find sources. In this method the background is computed from a global map of the detector; hence sources are not lost because their extended flux distribution increases the apparent background around them (see Gioia et al. 1990b for details). The flux for each source was converted from IPC counting rates with a Raymond-Smith thermal spectrum of 6 keV and corrected for absorption using the neutral hydrogen values from the survey of Stark et al. (1984). Most of the sky was observed through a small range of $N_{\rm H}$, resulting in a negligible bias (see Maccacaro et al. 1988 and Zamorani et al. 1988). *K*-corrections were small for this sample and were calculated assuming for simplicity a power-law spectrum with energy index of 0.5, which approximates a 6 keV thermal spectrum in the 0.3–3.5 keV band. The largest correction accounts for the finite size of the detection cell. This correction varies with redshift and must be included in any calculation involving the flux of the sources. The EMSS sample of clusters is in fact a surface brightness–limited sample rather than a flux-limited sample. Thus what we and other authors who have used the cluster sample (see Gioia et al. 1990b; Donahue, Stocke, & Gioia 1992; Henry et al. 1992) have attempted to do is to take into account the spatial variations of the X-ray surface brightness in order to correct the surface brightness–limited sample to a flux-limited sample. To do this, an estimate of the spatial distribution of X-ray flux for distant clusters is derived based upon the observed structure of nearby clusters. Since cluster X-ray emission is extended and comparable to the size of the detection cell, this correction is significant at low redshift and becomes less important, but not negligible, at high redshift (see values for detection cell flux and corrected total flux in cols. [5] and [6] of Table 1). Gioia et al. (1990b) and Henry et al. (1992) have described in detail the prescription for correcting this selection effect (see also the discussion in Donahue et al. 1992).

Briefly, a $\beta = 2/3$ model for cluster surface brightness distribution is adopted. The surface brightness is then integrated over the square 2′.4 × 2′.4 detection cell to calculate the fraction of total flux deposited in the detection cell. A core radius, observationally determined from a large number of clusters observed by nonimaging, large beam experiments and which have IPC imaging data, is then used to correct the observed luminosity to the total "true" luminosity for the flux lost outside the detection cell. The luminosities in column (7) of Table 1 have been computed adopting this correction.

Another point worth mentioning is the presence of cooling flow clusters in the sample. It has been suggested (Pesce et al. 1990; Edge, Stewart, & Fabian 1992) that most of the clusters found in the EMSS contain cooling flows given the point-source detection algorithm used in the survey. Donahue et al. (1992) have shown that some non–cooling flow EMSS clusters have small core radii, thus implying that the sample is not necessarily dominated by cooling flow clusters. Besides, Donahue et al. (1992) suggest that many clusters with large core radii may have low luminosities and thus would not be detected in X-ray imaging surveys even if they were more compact. More compelling evidence that the EMSS does not miss clusters which are not cooling flow clusters is given by the agreement between the X-ray luminosity function of the EMSS clusters with redshifts between 0.14 and 0.2, and the luminosity function derived by earlier studies (Piccinotti et al. 1982) which use large-beam, non–imaging detector fluxes. The agreement seems to indicate that this bias is not present in our sample, or at least it is at work in the same manner in the non-imaging data (see also Henry et al. 1992 and Donahue et al. 1992 for an extensive discussion of this last point).

The X-ray emission of clusters possessing enough counts to allow a meaningful analysis of their morphologies ranges from smooth extended features to more complex structures with several subcondensations (X-ray isocontour maps for sources with more than 100 counts are published in Gioia et al. 1984, Gioia et al. 1987, and Gioia et al. 1990a). The X-ray emission is often centered on a bright, optically dominant galaxy. However, there are also several cases where there are two approximately equally bright galaxies and the cluster appears to be irregular, and many cases where no dominant galaxy is visible (see CCD images in this paper) and the cluster is not rich. In fact, both rich clusters and poor groups of galaxies, with or without cD galaxies, seem to be selected in X-rays. Optical selection is based on high apparent galaxy concentration and thus would select only rich clusters in the absence of confusion.

The resulting sample of 104 clusters is given in Table 1 with the above described corrections applied. Columns list the observed and derived parameters for each cluster as follows:

Col. 1.—EMSS name. Those clusters preceded by an asterisk make up the 41 cluster are survey sample whose images are presented in Figures 2.1–2.41.

Col. 2.—Other name.

Col. 3.—Right ascension and declination in 1950.0 coordinates of the cluster optical position. Most of these positions were measured on the POSS or SRC J plates (Stocke et al. 1991) and are accurate to $\pm 5''$. When the brightest cluster member has been detected in radio, then the VLA position is given accurate to $\pm 1''$.

Col. 4.—Redshift of the cluster (± 0.003). Those redshifts enclosed by parentheses are tentative values.

Col. 5.—X-ray flux, in units of 10^{-13} ergs cm^{-2} s^{-1} (0.3–3.5 keV) in the $2'.5 \times 2'.4$ detection cell with correction only for vignetting and mirror scattering.

Col. 6.—Corrected X-ray flux (same units).

Col. 7.—Corrected X-ray luminosity in units of 10^{44} ergs s^{-1} (0.3–3.5 keV).

Col. 8.—Radio flux at 6 cm or a 5 σ upper limit.

Radio observations at 6 cm with the VLA in a variety of telescope configurations were performed for the 98 clusters in the declination range $\delta \geq -43°$. A detection rate of 50% is reached with most of the radio detections unresolved and coincident with the brightest galaxy in the cluster. There are, however, a few resolved structures which have been published in Gioia et al. (1987). Table 2 presents the radio position and 6 cm flux for all the radio sources detected in the cluster fields and their association with the cluster galaxies as indicated in the Comments column.

2.2. *The EMSS Distant Cluster Sample for the Arc Survey*

The 41 cluster subsample chosen for the gravitationally lensed arc survey (Luppino et al. 1993, 1994), whose optical images are presented here, is subject to the following additional restrictions. First, the sources must have a declination $\delta \geq -40°$ to be observable from Mauna Kea. Second, the fluxes of the sources in the $2'.4 \times 2'.4$ detection cell (flux in col. [5] of Table 1) must be $F_x^{\rm Det} \geq 1.33 \times 10^{-13}$ ergs cm^{-2} s^{-1} after converting from IPC counting rates with a thermal spectrum of 6 keV temperature and correcting for the galactic absorption in the direction of each source, but with no IPC point response function correction applied. These two selection criteria restrict the number of unidentified sources to only nine of 733 sources, an identification rate of 98.8%. Third, the redshift of the cluster must be $z \geq 0.15$ to ensure a distant sample for which at least 1 Mpc $\times$ 1 Mpc would be imaged onto our $7'.5 \times 7'.5$ CCD field. Fourth, the X-ray luminosity must be greater than $L_x = 2 \times 10^{44}$ ergs s^{-1} to select for deep potential wells which are most likely to exhibit gravitational lensing. These selection criteria result in a subsample of 41 clusters which are identified with an asterisk in Table 1.

2.3. *The Remaining EMSS Unidentified Sources*

The nine still unidentified sources in the restricted EMSS catalog of 733 sources are given in Table 3. This list updates the one that appeared as Table 1 in Henry et al. (1992). One of the previously unidentified sources, MS 1610.4+6616, has been classified as a distant cluster and is included in our sample. Two other unidentified sources have been associated with active galactic nuclei (T. Maccacaro & A. Wolter, private communication). No plausible optical counterparts have been found in the IPC error circles of the nine sources in Table 3 despite optical observations of the candidates visible on the POSS, or on moderate resolution CCD images that we have acquired during the identification process of the 835 EMSS sources. The IPC has a positional accuracy of only $\sim 50''$ (90% confidence radius) so we have obtained *ROSAT* PSPC observations for seven of the unidentified sources. Reduction of the *ROSAT* data is still under way, but from an inspection of the new X-ray data there are no more than two sources which could be identified with clusters of galaxies (Gioia et al. 1994). Deeper imaging and/or spectroscopy is necessary to identify unambiguously these remaining nine sources. The small number of unidentified sources which could be associated with galaxy clusters makes the EMSS cluster sample a well-defined, homogeneous, and statistically reliable list of clusters which can be used for cosmological studies.

3. *Observations and Data Reduction*

The optical observations were carried out during the period from 1992 May to 1993 November using a thinned Tektronix 2048 $\times$ 2048 pixel CCD mounted at the f/10 focus of the University of Hawaii 88 inch (2.24 m) telescope on Mauna Kea. The image scale was $0''.22$ pixel^{-1}, and the resulting field of view was $7'.5 \times 7'.5$. Images were taken through (Johnson) *B* and (Kron-Cousins) *R* filters. The data were calibrated using the photometric standards of Landolt (1992). Exposures ranged from tens of minutes for the relatively bright, nearby clusters to several hours for the most distant clusters. All the data were taken with the same instrument configuration—telescope, filters and detector. For the most part, these data are of superior quality. The median seeing for the entire 41 cluster sample is $0''.8$ FWHM (see Fig. 1).

In order to build up our long exposures, we took a number of short exposures (typically 600s or 900s each) with the telescope shifted between exposures, allowing us to assemble a median-filtered stack of the disregistered images to use for flattening the data. These multiple exposures were then shifted into registration and combined while being cleaned of cosmic rays.

We chose the *B* and *R* bandpasses for the following reasons. The *R* bandpass is ideal for observing the distant clusters in the redshift range spanned by the EMSS sample. The center wavelength of the *R* filter occurs at the peak of the CCD quantum efficiency and the night sky is darker than a redder bandpass such as *I*. Although gravitationally lensed arcs are known to be relatively blue, they are still more easily detected in the *R*-band

TABLE 1

EMSS X-RAY-SELECTED GALAXY CLUSTER SAMPLE

(1) EMSS Name	(2) Other Name	(3) Optical Coordinates (1950.0) R.A.			Dec.			(4) z	(5) X-ray Data F_x^{Det} $\times 10^{-13}$	(6) F_x^{Tot} $\times 10^{-13}$	(7) L_x $\times 10^{44}$	(8) F_R (6 cm) mJy
MS0002.8+1556		00	02	49.9	+15	56	24.3	.116	7.28	28.47	1.643	<0.9
MS0007.2−3532		00	07	14.5	−35	33	11.8	.050	3.96	48.22	0.517	<0.5
*MS0011.7+0837		00	11	45.5	+08	37	19.4	.163	11.60	33.10	3.769	80.3
MS0013.4+1558		00	13	20.9	+15	58	17.3	.083	3.59	20.83	0.616	<1.0
*MS0015.9+1609	CL0016+16	00	15	58.3	+16	09	34.0	.546	7.06	11.58	14.639	0.8
MS0026.4+0725		00	26	26.5	+07	25	37.0	.170	4.71	13.00	1.609	2.7
MS0037.8+2917	A77	00	37	48.1	+29	16	53.6	.069	18.64	139.00	2.838	5.3
MS0043.3−2531		00	43	17.5	−25	32	06.0	.112	2.26	9.16	0.493	1.8
MS0102.3+3255		01	02	21.3	+32	55	19.8	.080	7.74	47.11	1.294	1.4
MS0109.4+3910		01	09	18.2	+39	11	21.6	.208	1.86	4.45	0.824	9.1
MS0147.8−3941		01	47	53.2	−39	42	01.5	.373	1.47	2.66	1.581	<0.3
MS0159.1+0330	A293	01	59	12.0	+03	30	28.1	.165	2.96	8.38	0.977	260.0
MS0301.7+1516		03	01	43.3	+15	15	50.6	.083	1.93	11.18	0.330	<0.8
*MS0302.5+1717		03	02	29.4	+17	16	47.6	.425	2.15	3.75	2.879	<1.3
*MS0302.7+1658		03	02	43.2	+16	58	27.0	.426	3.75	6.54	5.043	3.3
MS0320.9−5322		03	20	47.6	−53	21	46.5	.071	5.69	40.82	0.883	
MS0353.3−7411	A3186	03	53	15.3	−74	10	39.2	.127	18.76	66.87	4.625	
*MS0353.6−3642	S400	03	53	38.3	−36	42	33.1	.320	6.25	11.99	5.244	1.2
MS0407.2−7123		04	07	06.4	−71	24	25.3	.229	4.68	10.58	2.373	
MS0418.3−3844		04	18	20.8	−38	45	09.6	.350	1.49	2.74	1.433	<0.4
MS0419.0−3848		04	18	59.6	−38	49	01.2	.225	0.78	1.78	0.385	<0.5
*MS0433.9+0957		04	33	58.4	+09	57	36.7	.159	13.74	40.01	4.335	43.5
*MS0440.5+0204		04	40	33.8	+02	04	43.7	.190	10.19	25.91	4.007	4.9
MS0450.6−5602		04	50	36.7	−56	02	11.4	.094	2.42	12.02	0.456	
*MS0451.5+0250	A520	04	51	35.7	+02	50	34.7	.202	16.35	39.92	6.976	5.2
*MS0451.6−0305		04	51	40.5	−03	05	46.0	.55	9.51	15.57	19.976	<0.8
MS0508.8−4523		05	08	50.2	−45	23	00.8	(.20)	16.35	40.16	6.880	
MS0537.1−2834		05	37	06.8	−28	34	40.6	.254	1.02	2.17	0.599	<1.1
MS0620.6−5239		06	20	36.9	−52	40	01.7	.048	8.62	112.00	1.107	1230.0
MS0623.6−5238		06	23	40.6	−52	38	58.3	.074	2.00	13.52	0.318	
MS0624.3−5519		06	24	18.6	−55	19	17.6	.118	4.76	18.28	1.091	
MS0733.6+7003	A588	07	33	37.8	+70	03	39.1	.117	2.14	8.29	0.487	<0.6
*MS0735.6+7421	Zw1370	07	35	34.8	+74	21	37.4	.216	13.10	30.64	6.119	2.3
MS0810.5+7433		08	10	36.2	+74	33	25.2	.282	2.25	4.56	1.549	<0.9
*MS0811.6+6301		08	11	36.8	+63	02	21.3	.312	2.60	5.04	2.098	<0.8
MS0821.5+0337		08	21	33.7	+03	37	30.3	.347	1.39	2.58	1.328	<0.6
*MS0839.8+2938	Zw1883	08	39	53.3	+29	38	16.0	.194	13.23	33.18	5.348	5.6
MS0849.7−0521		08	49	46.3	−05	21	36.5	.192	2.96	7.46	1.179	7.1
MS0904.5+1651	A744	09	04	33.0	+16	51	15.0	.073	5.82	40.12	0.918	<1.4
*MS0906.5+1110	A750	09	06	30.1	+11	10	39.3	.180	15.72	41.56	5.769	<0.5
MS0955.7−2635		09	55	45.2	−26	35	56.2	.145	7.19	22.63	2.039	<0.7
MS1004.2+1238		10	04	12.7	+12	38	15.9	.166	2.79	7.84	0.925	2.3
*MS1006.0+1202	Zw2933	10	06	07.3	+12	02	20.4	.221	9.99	23.05	4.819	<0.6
*MS1008.1−1224		10	08	05.4	−12	25	07.4	.301	5.89	11.60	4.493	<0.8
MS1020.7+6820	A981	10	20	36.7	+68	20	03.7	.203	2.80	6.82	1.204	1.1
MS1050.7+4946		10	50	47.5	+49	45	54.4	.140	12.47	40.52	3.405	53.8
*MS1054.4−0321		10	54	26.9	−03	21	25.3	(.81)	2.11	3.27	9.016	6.1
MS1058.7−2227	A1146	10	58	48.0	−22	27	46.6	.141	12.10	39.06	3.329	2.9
MS1111.8−3754		11	11	49.8	−37	54	55.8	.129	17.23	60.34	4.325	<0.7
MS1125.3+4324		11	25	17.9	+43	24	09.5	.181	20.44	5.38	0.756	<0.6
MS1127.7−1418	A1285	11	27	52.3	−14	18	19.2	.105	13.52	58.92	2.786	<3.2
*MS1137.5+6625		11	37	36.2	+66	24	56.9	(.65)	1.89	3.01	5.375	<0.9
*MS1147.3+1103		11	47	18.2	+11	03	15.9	.303	2.99	5.87	2.304	6.1
MS1154.1+4255		11	54	11.6	+42	54	49.5	.174	3.57	9.69	1.258	9.8
*MS1201.5+2824		12	01	30.4	+28	23	47.1	.167	6.05	16.94	2.025	<1.0
MS1205.7−2921		12	05	43.1	−29	21	18.0	.171	2.86	7.85	0.984	4.4
*MS1208.7+3928		12	08	44.0	+39	28	19.0	.340	2.19	4.11	2.030	1.4
*MS1209.0+3917		12	09	00.6	+39	18	04.6	(.33)	2.81	5.33	2.493	4.6
MS1219.9+7542		12	19	56.9	+75	42	53.0	.240	2.36	5.19	1.281	1.9
*MS1224.7+2007		12	24	42.6	+20	07	30.0	.327	5.30	10.09	4.606	<0.7
*MS1231.3+1542		12	31	24.3	+15	42	28.4	.238	5.38	11.89	2.883	<0.6
*MS1241.5+1710		12	41	31.6	+17	10	06.7	.312	4.23	8.20	3.411	<0.7
*MS1244.2+7114	Zw5434	12	44	09.6	+71	14	15.1	.225	7.77	17.73	3.843	5.5
*MS1253.9+0456	Zw5587	12	53	54.1	+04	56	25.7	.230	6.16	13.88	3.143	<0.6
MS1305.4+2941	Zw5722	13	05	25.9	+29	41	47.0	.241	2.63	5.77	1.434	2.4
MS1306.7−0121		13	06	44.8	−01	21	23.3	.088	9.50	51.13	1.698	3.1
MS1308.8+3244		13	08	50.6	+32	43	59.5	.245	3.19	6.93	1.779	<3.2
MS1317.0−2111		13	17	02.2	−21	11	38.9	.164	4.63	13.14	1.515	<1.0
*MS1333.3+1725		13	33	21.7	+17	24	57.8	.460	3.52	6.00	5.404	<0.9
MS1335.2−2928		13	35	16.2	−29	29	19.2	.189	3.30	8.43	1.289	86.0
*MS1358.4+6245	Zw6429	13	58	20.9	+62	45	35.0	.327	12.23	23.27	10.624	3.8
MS1401.9+0437		14	01	56.8	+04	37	23.6	.230	1.72	3.87	0.876	<0.9
MS1409.9−0255		14	09	59.8	−02	55	07.7	.221	2.16	4.98	1.042	<1.0

TABLE 1—*Continued*

(1) EMSS Name	(2) Other Name	(3) Optical Coordinates (1950.0) R.A.			Dec.			(4) z	(5) X-ray Data F_x^{Det} $\times10^{-13}$	(6) F_x^{Tot} $\times10^{-13}$	(7) L_x $\times10^{44}$	(8) F_R (6 cm) mJy
MS1421.0+2955		14	20	59.2	+29	55	46.0	.261	2.26	4.75	1.384	<1.0
*MS1426.4+0158		14	26	26.7	+01	58	36.9	.320	4.42	8.47	3.707	<1.0
MS1454.0+2233	Zw7160	14	54	00.3	+22	33	15.0	.108	1.79	7.55	0.377	2.8
*MS1455.0+2232		14	55	00.5	+22	32	34.7	.259	26.44	55.87	16.029	1.9
*MS1512.4+3647		15	12	25.9	+36	47	26.7	.372	4.49	8.14	4.807	3.8
MS1520.1+3002		15	20	09.4	+30	03	16.7	.117	3.46	13.40	0.787	1.4
MS1522.0+3003	A2069	15	22	03.6	+30	03	52.1	.116	10.41	40.68	2.347	<1.2
MS1531.2+3118	A2092	15	31	14.1	+31	18	42.2	.067	2.97	23.28	0.444	12.6
MS1532.5+0130		15	32	29.4	+01	30	46.3	.320	1.96	3.75	1.641	<0.9
*MS1546.8+1132		15	46	52.0	+11	32	25.6	.226	5.90	13.44	2.937	<1.1
MS1558.5+3321	A2145	15	58	26.9	+33	21	40.7	.088	7.95	42.75	1.420	5.0
*MS1610.4+6616		16	10	31.1	+66	16	00.0	(.55)	2.24	3.66	4.701	<1.1
MS1617.1+3237		16	17	08.8	+32	37	52.6	.274	1.80	3.69	1.185	<0.9
*MS1618.9+2552	A2177	16	18	56.7	+25	53	22.3	.161	7.00	20.17	2.241	<0.9
*MS1621.5+2640		16	21	32.2	+26	41	06.4	.426	3.38	5.88	4.546	2.6
MS1754.9+6803	Zw8303	17	54	50.8	+68	03	51.6	.077	9.00	57.63	1.467	2.5
*MS1910.5+6736		19	10	29.8	+67	36	24.6	.246	7.81	16.94	4.386	<2.0
*MS2053.7−0449		20	53	44.0	−04	49	24.7	.583	2.48	4.01	5.775	<0.8
MS2124.7−2206		21	24	39.4	−22	07	15.2	.113	5.27	21.20	1.161	<0.5
*MS2137.3−2353		21	37	24.4	−23	53	17.6	.313	19.28	37.33	15.621	1.0
MS2142.7+0330		21	42	43.1	+03	30	40.0	.239	2.66	5.87	1.436	<0.9
MS2215.7−0404		22	15	41.3	−04	04	25.2	.090	6.58	34.44	1.196	<0.9
MS2216.0−0401		22	16	04.7	−04	01	51.9	.090	10.65	55.69	1.935	<0.9
*MS2255.7+2039	Zw8795	22	55	40.6	+20	39	04.2	.288	2.87	5.76	2.041	<0.7
*MS2301.3+1506	Zw8822	23	01	17.1	+15	06	49.8	.247	5.82	12.61	3.291	2.5
MS2311.2−4259	S1101	23	11	12.1	−43	00	00.3	.058	93.19	898.10	12.963	46.4
MS2316.3−4222	S1111	23	16	21.1	−42	23	15.4	.045	24.15	348.80	3.031	540.0
*MS2318.7−2328	A2580	23	18	47.5	−23	28	55.1	.187	17.76	45.69	6.844	14.6
MS2318.9−4210	A3998	23	18	53.8	−42	10	14.8	.089	21.32	113.10	3.842	3.5
MS2348.0+2913		23	48	03.5	+29	13	01.2	.095	14.72	72.06	2.789	14.1
MS2354.4−3502	A4059	23	54	25.9	−35	02	15.8	.046	3.10	43.14	0.392	110.0
MS2356.9−3434		23	56	53.2	−34	35	04.2	.115	1.82	7.19	0.408	<0.5

Notes to Table 1

Cluster	Notes to Table 1
MS0002.8+1556	Loose cluster with dominant galaxy, extended in X-rays (contour map in Gioia *et al.* 1990a).
*MS0011.7+0837	The dominant galaxy is a cD radiogalaxy with the classical double-lobed structure.
MS0013.4+1558	This cluster is clumpy in X-rays with some of the peaks associated with the galaxies. An X-ray contour map has been presented in Gioia *et al.* (1984). The two bright stars in the area (a 16th magnitude M star and a 12th magnitude G star) may contribute part of the emission, however they are both too faint to be the majority of the total X-ray flux.
*MS0015.9+1609	This is a well known distant cluster (often called Cl 0016+16) with an optical linear structure. It is extremely rich and it was first discovered by R. Kron (see Koo 1981). Pointed IPC observations were reported by White, Silk and Henry (1981) but the presence of this cluster in the EMSS survey is due to its detection in a separate IPC exposure of another distant cluster also discovered by Kron but at a different redshift than this one. The redshift comes from Dressler and Gunn (1992) who also give spectra of many of the cluster members. MS0015.9+1609 is one of the brightest X-ray emitting clusters, and its high redshift has made it a popular object for cosmological studies. Koo (1981) first noticed that Cl 0016+16 was quite red and was an example of a high-z cluster that did not exhibit the Butcher-Oemler effect. Spectroscopic observations, however, revealed a number of "E+A" active galaxies indicating a so-called "active fraction" consistent with other distant clusters.
MS0026.4+0725	Rich and compact cluster. The brightest galaxy has moderate [O II] λ 3727 emission and radio emission (Stocke *et al.* 1991). Iso-contour X-ray map presented in Gioia *et al.* (1984).
MS0037.8+2917	A starburst galaxy at z=0.076 is present within the X-ray contours of this cluster that is identified with Abell 77. Given the typical X-ray luminosities of starburst galaxies, this galaxy does not contribute significantly to the X-ray emission observed.
MS0043.3−2531	Compact group of galaxies elongated in the EW direction. An optical study of this cluster by Garilli *et al.* (1992) shows an irregular poor cluster, much similar to a loose group, with a blue-galaxy fraction of 26%.
MS0102.3+3255	The bright dominant galaxy has no emission lines and is radio emitting.
MS0109.4+3910	Medium-distant compact and rich cluster.
MS0147.8−3941	Distant loose cluster. Its low X-ray luminosity excludes it from the arc survey sample.
MS0159.1+0330	Abell 293 (z=0.165) contains the strong radio galaxy PKS0159+034. X-ray emission consists of three portions (see Gioia *et al.* 1984 for the X-ray iso-contour map and finding chart of the area), two of which are associated with Abell 293 (NE and NW). The southern emission is likely due to a background QSO at z=1.897 and contributes only a small fraction to the total X-ray flux.
MS0301.7+1516	Poor, irregular nearby cluster.
*MS0302.5+1717	This cluster and MS0302.7+1658 below were detected in an IPC image whose target was Cl 0303+1706, a distant cluster at a similar redshift (z=0.4181) discovered optically by Gunn, Hoessel & Oke (1986; see also Dressler and Gunn 1992). Fabricant, Bautz & McClintock (1994) showed that the three clusters are not gravitationally bound. Photometric and spectroscopic data for both EMSS clusters are given in Fabricant, Bautz & McClintock (1994).
*MS0302.7+1658	Compact cluster, the brightest galaxy shows weak [O II] λ 3727 emission and radio emission. Mathez *et al.* (1992) discovered the "straight" arc between the two brightest ellipticals and obtained spectra for 4 galaxies and photometry for 39 galaxies. Giraud (1992) published additional data. In our deep image in $0''.6$ seeing we easily see the giant lensed arc. See also previous note.

TABLE 1—*Continued*

Cluster	Notes to Table 1
MS0320.9−5322	X-ray emission comes from several condensations (iso-contour map presented in Gioia *et al.* 1990a). NW blob sits on dominant galaxy which has weak [O II] λ3727 emission (Stocke *et al.* 1991).
*MS0353.3−7411	Abell 3186, extended X-ray structure (map in Gioia *et al.* 1990a). Garilli *et al.* (1992) compare the X-ray contours with the optical isopleths and point out the similarity of the two morphologies (both slightly elongated in the NW-SE direction) suggesting a certain degree of coupling between luminous matter and hot gas.
MS0353.6−3642	The optical CCD image shows a compact cluster with the three central galaxies embedded in a common envelope. Photometry for this cluster is given in Garilli *et al.* (1992), who compute a richness parameter $N_{0.5}$=28 resulting in a cluster richer than expected in the X-ray-luminosity-$N_{0.5}$ relation (Bahcall 1980) and similar to MS1358.4+6245 (see Luppino *et al.* 1991). They quote a 29% fraction of blue galaxies in this cluster.
MS0407.2−7123	This cluster appears to be very rich in a deep CCD image taken at LCO 40″ telescope (Donahue, private communication).
MS0418.3−3844	Poor cluster, no dominant galaxy.
MS0419.0−3848	Poor cluster, central galaxy has moderate [O II] λ3727.
*MS0433.9+0957	Several bright galaxies, none dominant. Loose, rather poor cluster. Note this is the lowest redshift object in our 41 cluster subsample.
*MS0440.5+0204	Poor cluster with a very compact, multiple-nucleus central galaxy that could be a forming cD galaxy. A circular gravitational arc structure surrounds the cD envelope. Luppino *et al.* (1993) compute a lower limit to the mass of the core of $1.0 \times 10^{14} M_{\odot}$ from the simple lensing geometry. Donahue, Stocke & Gioia (1992) report extended H_{α} emission coincident with the core of the cluster, suggesting the presence of a large cooling flow—an interpretation supported by the presence of radio emission from the cD.
MS0450.6−5602	Compact, poor group.
*MS0451.5+0250	Abell 520. There is not a well defined optical center in this cluster but several galaxy condensations are visible. The X-ray source was detected near the edge of the IPC frame with the observed X-ray emission associated with a tight clump of galaxies at z=0.202. A more detailed analysis of the X-ray emission indicates that it may extend an additional 2 arcmin to the NE. If so, a portion of this source may be due to a poor cluster in that vicinity at a slightly higher redshift (z=0.22).
*MS0451.6−0305	Distant cluster, given its redshift (S. Morris, private communication) this is the most X-ray luminous cluster in the EMSS. The optical image reveals a very rich, compact cluster with a giant arc to the East of the brightest galaxy.
MS0508.8−4523	Optical spectrum has poor S/N. The two central galaxies seem merged in an SRC J plate. X-ray emission is extended, iso-contour map given in Gioia *et al.* (1990a).
MS0537.1−2834	The NE of two central galaxies has strong [O II] λ3727 emission but no radio emission.
MS0620.6−5239	Contains the powerful radiosource PKS0620−526. The X-ray structure is extended with several subcondensations. The X-ray map is presented in Gioia *et al.* (1984).
MS0623.6−5238	Field heavily obscured by Canopus (see finding chart in Gioia *et al.* 1984). The cluster classification is based upon what little can be seen of this field and is, therefore, tentative.
MS0624.3−5519	The dominant galaxy, ESO 161−5, has a red nucleus and a blue envelope. X-ray iso-contour map presented in Gioia *et al.* (1990a).
MS0733.6+7003	Abell 588, dominant galaxy present, quite rich.
*MS0735.6+7421	X-ray extended, the brightest galaxy has strong [O II] λ3727 emission and is radio emitting (Stocke *et al.* 1991). Optical morphology shows a moderately poor cluster with a large cD galaxy.
*MS0811.6+6301	Possible background cluster present at z=0.49. CCD image reveals a bright central galaxy with a number of smaller, nearby companions and a loose grouping of other galaxies in the background.
*MS0839.8+2938	The brightest galaxy in this compact cluster has extremely strong [O II] and Hα emission with equivalent widths and line ratios similar to those of cooling flow clusters. The peak of the X-ray emission is consistent with the position of the brightest cluster galaxy. A multi-waveband study of the cluster has been published in Nesci *et al.* (1989). High resolution ROSAT observations (Nesci *et al.* 1994) show three main peaks of emission. The emission is centered on the dominant galaxy and both the ellipticity and the position angle are very similar to those of the galaxy. The CCD image shows a field whose outer parts contain many spirals and clearly interacting systems, while the core is compact.
MS0849.7−0521	X-ray iso-contour map presented in Gioia *et al.* (1990a).
MS0904.5+1651	This cluster is identified with Abell 744. The cluster is dominated by a normal giant elliptical and is extended in X-rays. The iso-contour map has been published by Kurtz *et al.* (1985) who also present optical data for the cluster galaxies. The spatial distribution of redshifts is peculiar with the dispersion within the 150 kpc core radius being much greater than outside, in this Abell 744 is similar to the nearby cluster Abell 1060 (Hydra I; Richter & Huchtmeier 1983).
*MS0906.5+1110	In the IPC image the X-ray emission from this source largely overlaps with the X-ray emission of the source MS0906.3+1111, identified with a Seyfert galaxy at nearly the same redshift as the cluster. It is thus difficult to determine the true extent of the cluster x-ray emission. X-ray iso-contour map presented in Gioia *et al.* (1990a). The optical image shows a dominant galaxy with a secondary nucleus to the SW.
MS0955.7−2635	The central, non-dominant galaxy has weak [O II] λ3727 emission. The X-ray emission is extended, see the iso-contour map in Gioia *et al.* (1990a).
MS1004.2+1238	The central dominant cluster galaxy in this loose cluster has strong [O II] λ3727 emission and is radio emitting (Stocke *et al.* 1991).
*MS1006.0+1202	In this rich and compact cluster four arcs have been discovered by Le Fèvre *et al.* (1994). The field is only ∼ 10′ from Regulus and is heavily contaminated by scattered light, especially in the blue. An X-ray iso-contour map is presented in Gioia *et al.* (1990a).
*MS1008.1−1224	Very rich cluster, slightly extended in X-rays, see iso-contour map in Gioia *et al.* (1990a). The cluster has a circular distribution of galaxies surrounding a NS-elongated core. There is a secondary clump of galaxies to the N. Some gravitationally lensed arcs have been reported by Le Fèvre *et al.* (1994).
MS1020.7+6820	Abell 981, rich and loose cluster, three radiosources were detected in this field (see Table 2). None of them is on the brightest cluster galaxy.
MS1050.7+4946	The central dominant galaxy is also radioemitter, not a rich cluster.
*MS1054.4−0321	Extremely rich, very distant cluster. A very preliminary redshift of ∼ 0.81 is determined from Ca II break only (Stocke, private communication). If confirmed, this will be the most distant cluster in the EMSS catalog. The size and brightness of the cluster galaxies on the CCD image are consistent with the assumed redshift. The central galaxy is a radiosource.

TABLE 1—*Continued*

Cluster	Notes to Table 1
MS1058.7−2227	Abell 1146, a rich cluster with a dominant galaxy. The X-ray emission is extended and shows some clumpiness. It is centered on the cD galaxy, see X-ray iso-contour map in Gioia *et al.* (1990a).
MS1111.8−3754	Redshift determination comes from nine galaxies, a dominant bright galaxy is present. X-ray emission is extended but the source is detected at the edge of the IPC so no iso-contour map was produced.
MS1125.3+4324	The two brightest galaxies in this loose group have very strong [O II] λ3727 emission. They also have Hα emission extended on a scale comparable to their broad-band image (Donahue, Stocke & Gioia 1992). This source was previously classified in Stocke *et al.* (1991) as a cooling flow galaxy. Due to the presence of a few other galaxies, this source is now classified as a poor cluster.
MS1127.7−1418	The source is identified with Abell 1285. As in the case of MS0353.3−7411 (=Abell 3186), previously described, there is a very tight similarity between the optical and the X-ray morphologies. They are both elongated in the NW-SE direction along the axis connecting the 2 brightest cluster galaxies. The X-ray iso-contour map can be found in Gioia *et al.* (1990a).
*MS1137.5+6625	This cluster of galaxies has no spectroscopic redshift determination as yet but it is likely to be at a similar redshift (z = 0.65) as the target of the IPC observation, QSO 3C263 located ~ 20′ to the S, based upon CCD photometry (Stocke, private communication).
*MS1147.3+1103	Rich, elongated cluster with an elongated cD.
MS1154.1+4255	Rather sparse and very poor group of galaxies.
*MS1201.5+2824	Dominant galaxy present in this moderately rich, compact cluster. Abell 1455 is about 8′ away.
*MS1208.7+3928	Compact, rich cluster near a very bright star.
*MS1209.0+3917	This source was originally classified as a "cooling flow galaxy" by Stocke *et al.* (1991) on the basis of the very strong [O II] λ3727 emission exhibited by the radiogalaxy 40″ SE (the most southern of three objects) of the elongated object at the center of the optical CCD image. This source could actually be a very distant cluster but additional spectroscopic work is needed. At this time we consider the classification and ID very uncertain.
MS1219.0+7542	Poor cluster with a dominant galaxy showing a weak [O II] λ3727 emission.
*MS1224.7+2007	The brightest galaxy has very strong [O II] λ3727 emission . This cluster does not appear very rich in the CCD image, but the images of this cluster were taken through clouds.
*MS1231.3+1542	Rich, binary cluster elongated in the NW-SE direction. Both galaxies are of comparable brightness.
*MS1241.5+1710	Rich, loose cluster. No dominant galaxy.
*MS1244.2+7114	Similar to MS0440.5+0204 in being a poor cluster with a central, multiple-nucleus cD galaxy (up to six nuclei in a common envelope). The cD galaxy has a 5.5 mJy source and strong [O II] λ3727 emission. The halo of light that envelopes the nuclei is not symmetrical about any major nuclear condensation nor is it elliptical in shape (R. Schild private communication). This supports the idea that this represents an early stage in the formation of the cD galaxies before they would become relaxed.
*MS1253.9+0456	Very rich cluster with a bright cD elongated NS along with the cluster.
MS1305.4+2941	This cluster lies in SA 57. The redshift for the brightest galaxy, a member of the Zwicky cluster Zw 1305.4+2941 has been measured by H. Spinrad (see Katgert *et al.* 1983).
MS1306.7−0121	Poor cluster with dominant central galaxy. X-ray iso-contour map presented in Gioia *et al.* (1990a).
*MS1333.3+1725	This source is tentatively identified with a distant, poor cluster of galaxies. A spectrum of the brightest galaxy is at low S/N and consistent with z=0.465. Additional spectroscopic data are needed to confirm.
*MS1358.4+6245	An optical and X-ray study of this cluster has been presented in Luppino *et al.* (1991). They find that the cluster exhibits the Butcher-Oemler effect with a photometric blue galaxy fraction of 18%. Fabricant, McClintock & Bautz (1991) present a number of spectra of ~70 galaxies in the core of the field. They find a specroscopic active galaxy fraction of 17%.
MS1401.9+0437	Loose cluster. No dominant galaxy present.
MS1409.9−0255	Poor cluster, no dominant galaxy present.
*MS1426.4+0158	Three galaxies in a common envelope at the center of the cluster. The bright galaxies visible in the CCD image are at a lower redshift, maybe two clusters in projection here. Field contains a number of spirals and possibly interacting systems.
MS1454.0+2233	Compact poor cluster.
*MS1455.0+2232	Poor cluster with one and possibly two bright ellipticals. The galaxy to the E is the brighter and is a radio emitter. It has strong [O II] λ3727 emission with an equivalent width of 60Å (Mason *et al.* 1981). An apparent gravitational arc is located slightly to the NE of this galaxy (see Le Fèvre *et al.* 1994). In Donahue (1990) this cluster has the strongest emission line flux (Hα and [N II]) of their survey, signifying a possible cooling flow.
*MS1512.4+3647	Centrally condensed cluster at the X-ray position. The central galaxy image is highly structured. There is a bright, blue, slightly-elongated (EW) object in the NW section of the core. Filamentary, blue structure is present in the central envelope.
MS1522.0+3003	An optical and X-ray study of Abell 2069 has been published in Gioia *et al.* (1982), where an X-ray iso-contour map is also presented. The cluster shows multiple condensations in both the X-ray emission and the galaxy surface density and thus the system as a whole does not appear relaxed. The close correspondence between the gas and the galaxy distributions seems to indicate that the galaxies in this system do map the mass distribution. A possible blue arc was discovered by Donahue, Stocke & Gioia (1992) North of the two central brightest galaxies. However, this cluster is at too low redshift to enter our 41 cluster sample.
MS1531.2+3118	Abell 2092, complex X-ray structure, iso-contour map presented in Gioia *et al.* (1990a). Redshift determination by Hoessel, Gunn & Thuan (1980).
MS1532.5+0130	A Seyfert galaxy at z=0.074 is also present in this field and is given as secondary identification by Stocke *et al.* (1991).
*MS1546.8+1132	Rich, elongated cluster with a giant cD.
*MS1610.4+6616	This source was previously unidentified. The CCD image shows a very distant and condensed cluster. The spectroscopic data that we are acquiring are not yet conclusive for the determination of the redshift, but the cluster is certainly at z>0.5.
MS1617.1+3237	cD galaxy present.
*MS1618.9+2252	Also Abell 2177. This rich, nearby cluster has a central galaxy with an asymmetric surface brightness with a fan-shaped brightening to the NW.
*MS1621.5+2640	X-ray emission of this distant cluster is resolved and possibly due to more than one optical counterpart. Only higher X-ray resolution data may unambiguously describe the structure. The cluster has been studied by Luppino & Gioia (1992) who reported the discovery of a gravitationally lensed arc around the second brightest galaxy which is also radioemitting.
MS1754.9+6803	Two brightest galaxies at the center of the cluster, slightly extended in X-rays.
*MS1910.5+6736	Moderately poor cluster that has some evidence of gravitational lensing (see Le Fèvre *et al.* 1994). The brightest galaxy has a double nucleus.

TABLE 1—*Continued*

Cluster	Notes to Table 1
*MS2053.7−0449	Until recently, this was the highest redshift cluster in the EMSS. Luppino & Gioia (1992) reported the discovery of a large arc to the NW of the center.
MS2124.7−2206	The brightest galaxy has a multiple nucleus. A starburst galaxy is also present in the same cluster but, based upon observed X-ray luminosities of starbursts, this galaxy is unlikely to contribute significantly to this source. X-ray iso-contour map is presented in Gioia *et al.* (1990a).
*MS2137.3−2353	This cluster has been studied by Fort *et al.* (1992) and Mellier *et al.* (1993) because of the presence of blue circular and radial arcs. Their lensing models indicate a very compact core radius of 50 kpc.
MS2142.7+0330	cD galaxy present.
MS2215.7−0404	and MS2216.0−0401 are two separate sources probably parts of the extended X-ray emission from a single cluster.
*MS2255.7+2039	The M star to the West of the central galaxy could contribute to the X-ray emission of this cluster.
*MS2301.3+1506	Rich cluster with a dominant cD.
MS2311.2−4259	Sersic 159-03. The nuclear region of the cD, ESO 291-G9, has been classified spectroscopically as LINER by Maia *et al.* (1987).
MS2316.3−4222	Southern Abell cluster with very bright cD galaxy. It contains the powerful radiosource PKS2316−423.
*MS2318.7−2328	Also Abell 2580. Bright, nearby cD galaxy in a rich cluster. Contains a possible lensed arc (see LeFèvre *et al.* 1994).
MS2318.9−4210	Abell 3998. A cD galaxy is present and the X-ray structure is extended (see iso-contour map in Gioia *et al.* 1990a).
MS2348.0+2913	Rich cluster, no dominant galaxy.
MS2354.5−3502	Very extended X-ray emission centered on the bright cD galaxy (ESO 349-G10 possible LINER in Maia *et al.* 1987) which is also PKS2354−350. X-ray iso-contour map presented in Gioia *et al.* (1987).

since their average $B - R$ color is roughly 1.3 (Soucail 1992). The additional B-band image is taken to recognize any gravitational arcs by their relative blue color compared to the red cluster galaxies.

4. *Results and Discussion*

Figures 2.1–2.41 show the resulting stacked CCD images obtained for the arc survey clusters. Additional parameters are given in each figure caption such as size and scale of the image, field of view at the redshift of the cluster (both in angular and linear units) plus any other interesting observational parameter (exposure time, seeing, etc.). For most of the clusters, we have extracted 1024 × 1024 or 1200 × 1200 subarrays centered on the cluster. These subarray images allow one to see at least the central 1 Mpc of the cluster. The coordinate grid surrounding each image is measured in arcseconds with the origin centered on the optical position given in Table 1. In all cases north is up and east is to the left as indicated at the upper left-hand part of the image.

A close inspection of the CCD images shows that the optical richness of X-ray–selected clusters is very diverse, ranging from poor groups of galaxies (e.g., MS 0043.3−2531 and MS 0433.9+0957) both with and without an optically dominant galaxy, to "extremely rich" clusters with hundreds of members (e.g., MS 0015.9+1609, MS 0451.6−0305, MS 1008.1−1224, MS 1054.4−0321, and MS 1358.4+6245). Different morphologies are also present: "binary" clusters with two central galaxies of comparable brightness (e.g., see MS 1231.3+1542); clusters with "linear" structures of galaxies as in the case of MS 0015.9+1609 and MS 1054.4−0321; loose, irregular (but nevertheless rich) clusters like MS 1241.5+1710; or compact clusters (MS 1201.5+2824 and MS 1208.7+3928). This classification is only subjective and qualitative at this time. Quantitative properties will be evaluated and presented in subsequent papers in this series.

Twenty Abell and 11 Zwicky clusters were "rediscovered" in the EMSS. An EMSS selection criterion causes the exclusion of Abell clusters with a distance class $D \leq 3$ from our sample, since most of the nearby clusters were chosen as targets of IPC observations and consequently were excluded from the survey of serendipitous X-ray sources. During this survey a new, distant cluster was added to the list, MS 1610.4+6616. This object was previously one of the unidentified sources. Even if the spectroscopic data in hand are not satisfactory for a firm redshift determination, the cluster is undoubtedly a distant one as can be clearly seen from the CCD image in Figure 2.33. On the

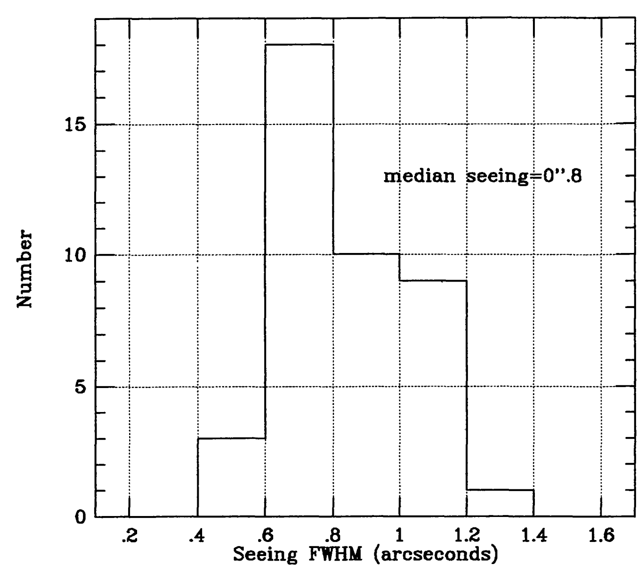

FIG. 1.—Histogram of the R-band seeing for the 41 EMSS cluster images shown in Fig. 2. The mean seeing is 0"88 FWHM, and the median seeing is 0"8 FWHM.

TABLE 2

RADIO SOURCES ASSOCIATED WITH EMSS CLUSTERS

(1) Name	(2) Radio Coordinates (1950.0) R.A.			Dec.			(3) Radio 6 cm flux (mJy)	(4) Comments
*MS0011.7+0837	00	11	45.4	+08	37	22.0	64.6	double radio source associated with the central galaxy
	00	11	46.5	+08	37	15.0	15.7	second component of double
*MS0015.9+1609	00	15	59.5	+16	10	03.5	0.8	on galaxy ~ 35″ to the NE
MS0026.4+0725	00	26	26.5	+07	25	37.0	2.7	on brightest galaxy
MS0037.8+2917	00	37	48.1	+29	16	53.6	5.3	on brightest galaxy
MS0043.3−2531	00	43	17.0	−25	31	40.5	1.8	not on brightest galaxy
	00	43	15.4	−25	31	58.0	8.4	double radio source associated with an AGN (z=0.86) to the West
	00	43	14.6	−25	32	01.5	3.9	second component of double
MS0102.3+3255	01	02	21.3	+32	55	19.8	1.4	on brightest galaxy
MS0109.4+3910	01	09	17.8	+39	11	24.6	9.1	on brightest galaxy
MS0159.1+0330	01	59	15.6	+03	28	42.6	260.0	PKS0159+034, radio position is 2.′3 SE of X−ray position
*MS0302.7+1658	03	02	43.2	+16	58	27.0	3.3	on brightest galaxy
*MS0353.6−3642	03	53	40.6	−36	42	23.1	1.2	on NE galaxy ~ 30″ away
	03	53	30.1	−36	43	04.6	3.6	on galaxy ~ 1.′73 to the East
*MS0433.9+0957	04	33	58.4	+09	57	36.7	2.0	on bright galaxy North
	04	33	59.5	+09	57	07.9	43.5	on bright galaxy North−East
*MS0440.5+0204	04	40	33.8	+02	04	43.7	4.9	on bright galaxy part of multiple nucleus, Luppino *et al.* 1993
	04	40	33.5	+02	04	28.7	1.8	on bright galaxy to the South
*MS0451.5+0250	04	51	24.2	+02	52	55.8	6.1	on spiral galaxy to the NW at the edge of CCD
	04	51	39.8	+02	50	43.8	5.2	on galaxy to the NE close to the center declination
	04	51	43.5	+02	50	09.8	3.6	on galaxy SE
MS0620.6−5239	06	20	37.3	−52	40	01.0	1230.0	PKS0620−526
*MS0735.6+7421	07	35	34.8	+74	21	37.4	2.3	on brightest galaxy
*MS0839.8+2938	08	39	53.3	+29	38	16.0	5.6	on brightest galaxy
MS0849.7−0521	08	49	47.3	−05	22	10.2	7.1	not on brightest galaxy
MS1004.2+1238	10	04	12.7	+12	38	15.9	2.3	on brightest galaxy
	10	04	10.3	+12	41	12.9	3.1	on galaxy to the NW
MS1020.7+6820	10	20	46.6	+68	21	10.6	1.1	not on brightest galaxy
	10	20	46.1	+68	20	57.6	0.9	not on brightest galaxy
	10	20	52.2	+68	19	09.6	4.3	not on brightest galaxy
MS1050.7+4946	10	50	47.5	+49	45	54.4	53.8	on brightest galaxy
*MS1054.4−0321	10	54	26.9	−03	21	25.3	6.1	on brightest galaxy
MS1058.7−2227	10	58	52.4	−22	27	12.4	2.9	on galaxy to the East
	10	58	39.0	−22	26	51.4	2.3	on object far away from center
*MS1147.3+1103	11	47	21.4	+11	04	13.3	6.1	on galaxy to the NE
MS1154.1+4255	11	54	11.6	+42	54	49.5	9.8	on brightest galaxy
MS1205.7−2921	12	05	43.1	−29	21	18.0	4.4	on brightest galaxy
	12	05	37.5	−29	23	01.5	1.8	no object visible on POSS
*MS1208.7+3928	12	08	44.0	+39	28	19.0	1.4	on brightest galaxy
*MS1209.0+3917	12	09	02.0	+39	17	34.6	4.6	on galaxy SE of optical CCD center
MS1219.9+7542	12	19	56.9	+75	42	53.0	1.9	on brightest galaxy
*MS1244.2+7114	12	44	09.6	+71	14	15.1	5.5	on brightest galaxy
MS1305.4+2941	13	05	25.9	+29	41	47.0	2.4	21 cm flux (Katgert *et al.* 1983), on brightest galaxy
MS1306.7−0121	13	06	44.8	−01	21	23.3	3.1	on brightest galaxy
MS1335.2−2928	13	35	16.2	−29	29	19.2	86.0	on brightest galaxy
*MS1358.4+6245	13	58	20.9	+62	45	35.0	3.8	on brightest galaxy
MS1454.0+2233	14	54	00.3	+22	33	15.0	2.8	on brightest galaxy
*MS1455.0+2232	14	55	00.5	+22	32	34.7	1.9	on brightest galaxy
*MS1512.4+3647	15	12	25.9	+36	47	26.7	3.8	on brightest galaxy
MS1520.1+3002	15	20	09.4	+30	03	16.7	1.4	not on brightest galaxy
MS1531.2+3118	15	31	13.7	+31	17	46.0	12.6	on second brightest galaxy
MS1558.5+3321	15	58	26.9	+33	21	40.7	5.0	on brightest galaxy
*MS1621.5+2640	16	21	31.9	+26	41	19.9	2.6	on second brightest galaxy, Luppino & Gioia (1992)
MS1754.9+6803	17	54	50.8	+68	03	51.6	2.5	on East of two central galaxies
*MS2137.3−2353	21	37	24.4	−23	53	17.6	1.0	on brightest galaxy (Stocke private communication)
*MS2301.3+1506	23	01	17.1	+15	06	49.8	2.5	on brightest galaxy
MS2311.2−4259	23	11	12.1	−43	00	00.3	46.4	on brightest galaxy
MS2316.3−4222	23	16	22.4	−42	23	40.0	540.0	on brightest galaxy, PKS2316−423
*MS2318.7−2328	23	18	47.5	−23	28	55.1	14.6	on brightest galaxy
	23	18	49.9	−23	29	15.1	1.6	on second brightest galaxy
MS2318.9−4210	23	18	53.8	−42	10	14.8	3.5	on brightest galaxy
MS2348.0+2913	23	48	04.2	+29	12	49.4	9.3	double radio source on brightest galaxy
	23	48	03.1	+29	13	03.4	4.8	second component of double
MS2354.4−3502	23	54	26.6	−35	02	26.0	110.0	PKS2354−350

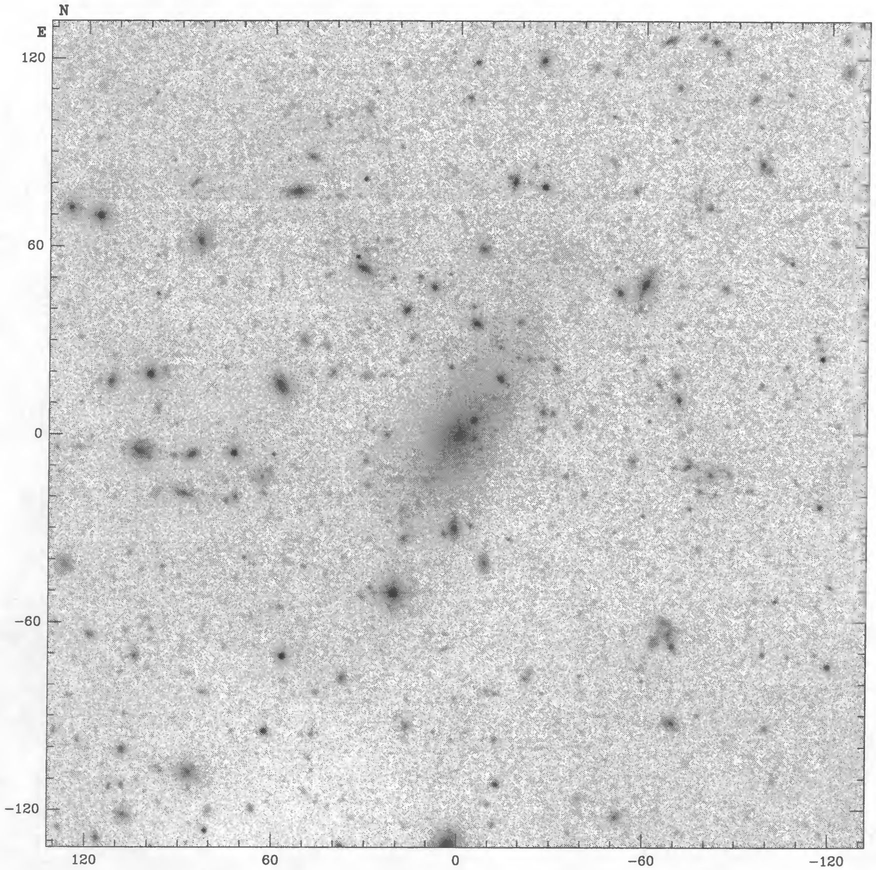

MS 0011.7+0837

Figure 2.1—CCD images of EMSS distant clusters

Redshift:	$z = 0.163$
X-ray luminosity:	$L_{x,44} = 3.77$
Image size/scale:	1200×1200 subarray at $0''.22$/pixel
Field of view:	$4'.4 \times 4'.4$
Scale at cluster redshift:	3.64 kpc/arcsecond
Field at cluster redshift:	0.96 Mpc $\times$ 0.96 Mpc
Total exposure time:	4800 s in R
Seeing:	$0''.65$

200 kpc

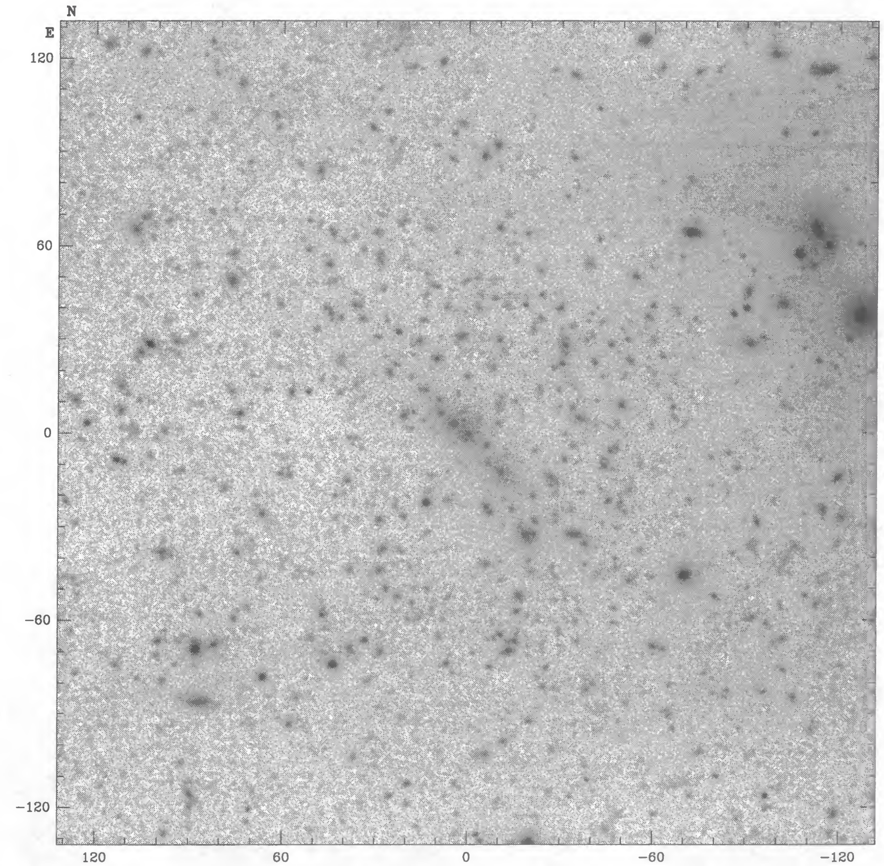

MS 0015.9+1609

Figure 2.2—CCD images of EMSS distant clusters

Redshift:	$z = 0.546$
X-ray luminosity:	$L_{x,44} = 14.64$
Image size/scale:	1200×1200 subarray at $0''.22$/pixel
Field of view:	$4'.4 \times 4'.4$
Scale at cluster redshift:	7.37 kpc/arcsecond
Field at cluster redshift:	1.9 Mpc $\times$ 1.9 Mpc
Total exposure time:	3.5 hours in B and 4 hours in R
Seeing:	$0''.8$

200 kpc

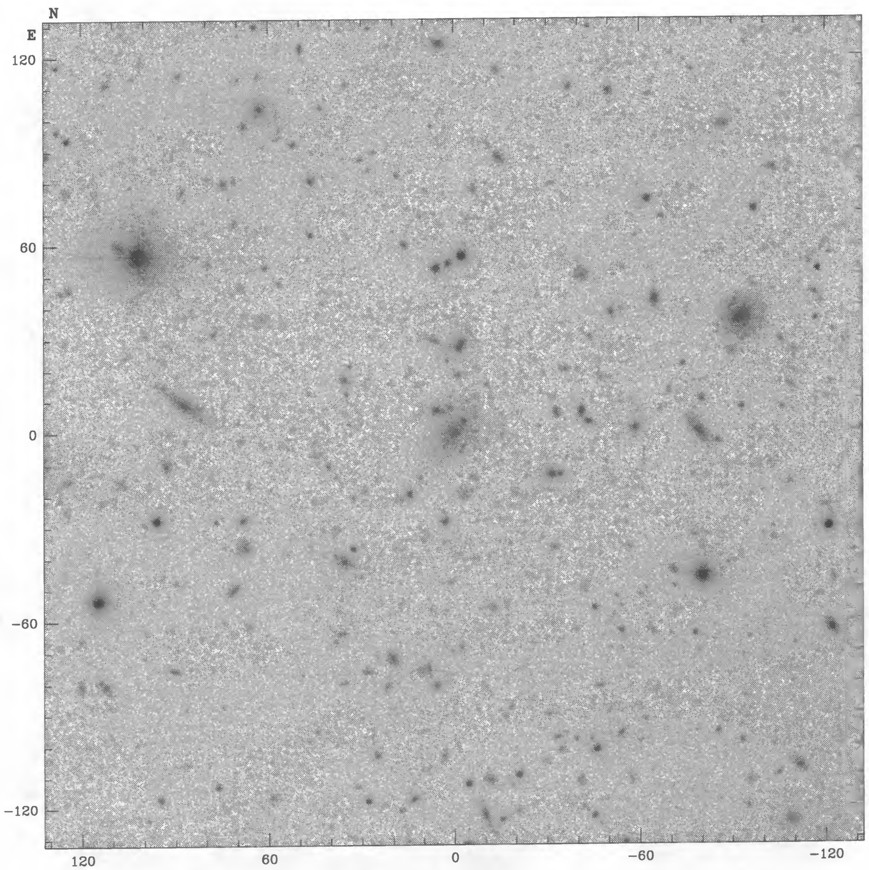

MS 0302.5+1717

Figure 2.3—CCD images of EMSS distant clusters

Redshift:	$z = 0.425$
X-ray luminosity:	$L_{x,44} = 2.88$
Image size/scale:	1200×1200 subarray at $0''.22$/pixel
Field of view:	$4'.4 \times 4'.4$
Scale at cluster redshift:	6.63 kpc/arcsecond
Field at cluster redshift:	1.75 Mpc $\times$ 1.75 Mpc
Total exposure time:	4500 s in R
Seeing:	$0''.8$

200 kpc

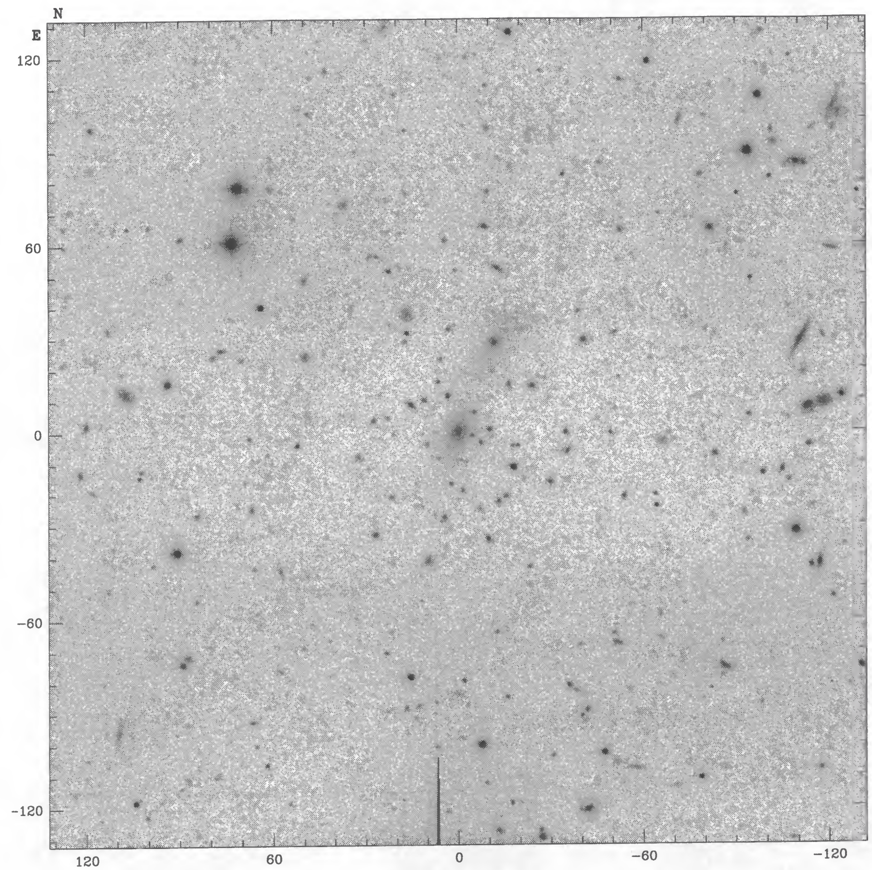

MS 0302.7+1658

Figure 2.4—CCD images of EMSS distant clusters

Redshift:	$z = 0.426$
X-ray luminosity:	$L_{x,44} = 5.04$
Image size/scale:	1200×1200 subarray at $0''.22$/pixel
Field of view:	$4'.4 \times 4'.4$
Scale at cluster redshift:	6.62 kpc/arcsecond
Field at cluster redshift:	1.75 Mpc $\times$ 1.75 Mpc
Total exposure time:	6000 s in R
Seeing:	$0''.6$
Notes:	Lensed arcs.

200 kpc

1994ApJS...94..583G

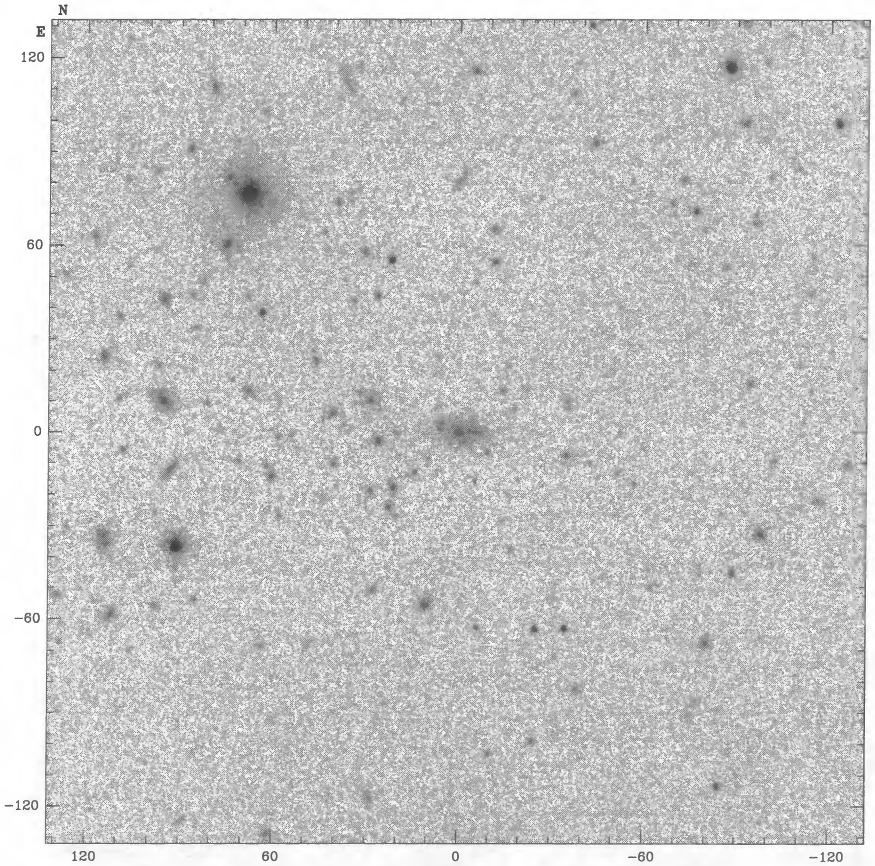

MS 0353.6−3642

Figure 2.5—CCD images of EMSS distant clusters

Redshift:	$z = 0.320$
X-ray luminosity:	$L_{x,44} = 5.24$
Image size/scale:	1200×1200 subarray at $0''.22$/pixel
Field of view:	$4'.4 \times 4'.4$
Scale at cluster redshift:	5.71 kpc/arcsecond
Field at cluster redshift:	1.5 Mpc $\times$ 1.5 Mpc
Total exposure time:	1800 s in R
Seeing:	$1''.1$

200 kpc

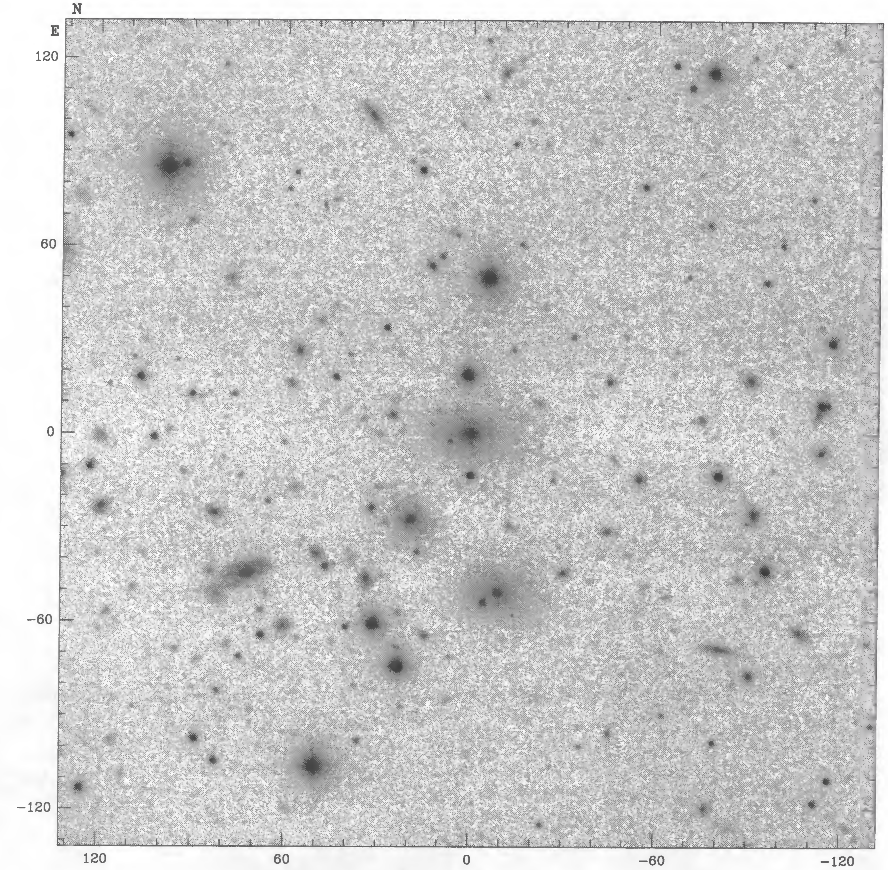

MS 0433.9+0957

Figure 2.6—CCD images of EMSS distant clusters

Redshift:	$z = 0.159$
X-ray luminosity:	$L_{x,44} = 4.33$
Image size/scale:	1200×1200 subarray at $0''.22$/pixel
Field of view:	$4'.4 \times 4'.4$
Scale at cluster redshift:	3.57 kpc/arcsecond
Field at cluster redshift:	0.94 Mpc $\times$ 0.94 Mpc
Total exposure time:	2400 s in R
Seeing:	$0''.9$

200 kpc

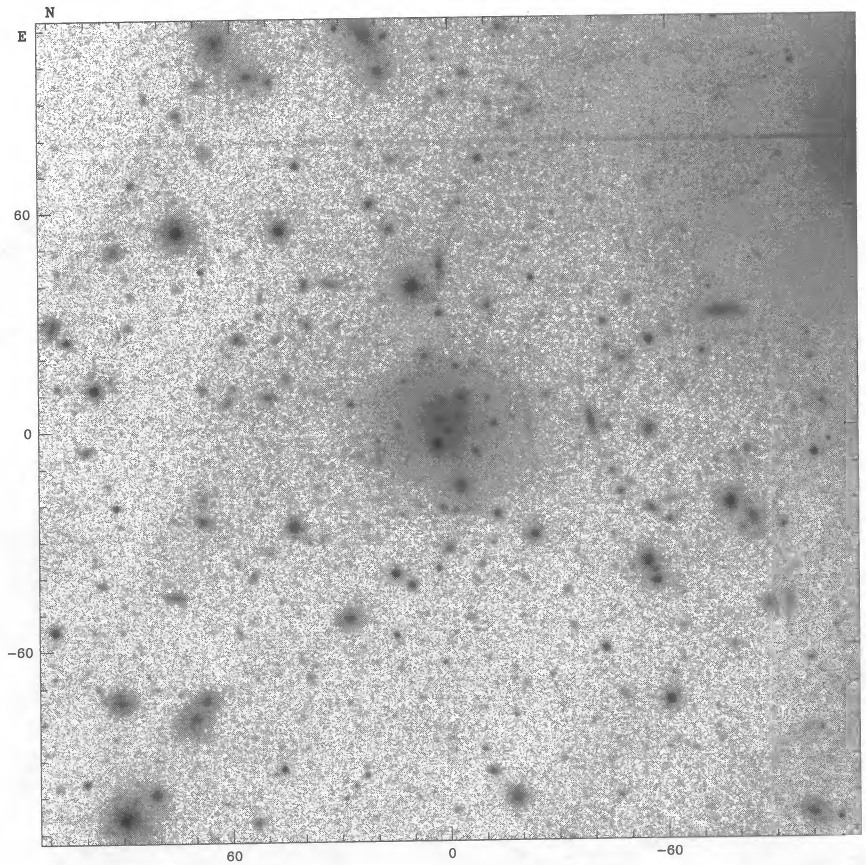

MS 0440.5+0204

Figure 2.7—CCD images of EMSS distant clusters

Redshift:	$z = 0.190$
X-ray luminosity:	$L_{x,44} = 4.01$
Image size/scale:	1024 × 1024 subarray at 0″.22/pixel
Field of view:	3′.8 × 3′.8
Scale at cluster redshift:	4.1 kpc/arcsecond
Field at cluster redshift:	0.92 Mpc × 0.92 Mpc
Total exposure time:	3300 s in R and 2700 s in B.
Seeing:	1″.1
Notes:	Lensed arcs; merging cD.

200 kpc

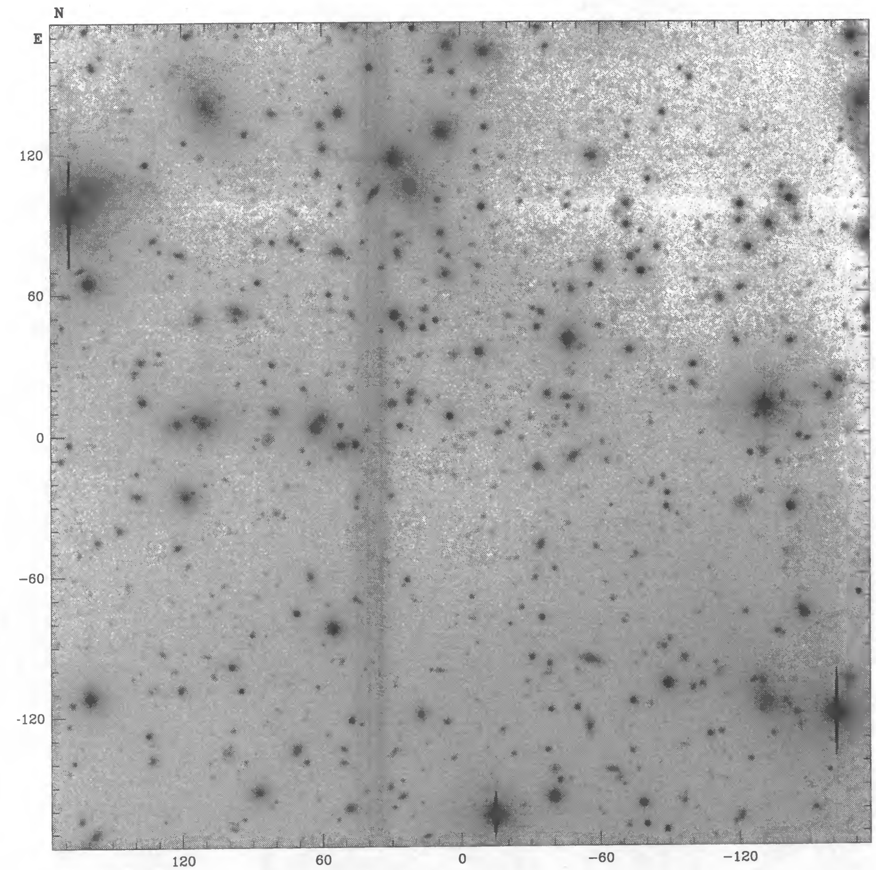

MS 0451.5+0250

Figure 2.8—CCD images of EMSS distant clusters

Redshift:	$z = 0.202$
X-ray luminosity:	$L_{x,44} = 6.98$
Image size/scale:	1600 × 1600 subarray at 0″.22/pixel
Field of view:	5′.9 × 5′.9
Scale at cluster redshift:	4.25 kpc/arcsecond
Field at cluster redshift:	1.5 Mpc × 1.5 Mpc
Total exposure time:	6300 s in R
Seeing:	0″.8
Notes:	Scattered light contamination.

200 kpc

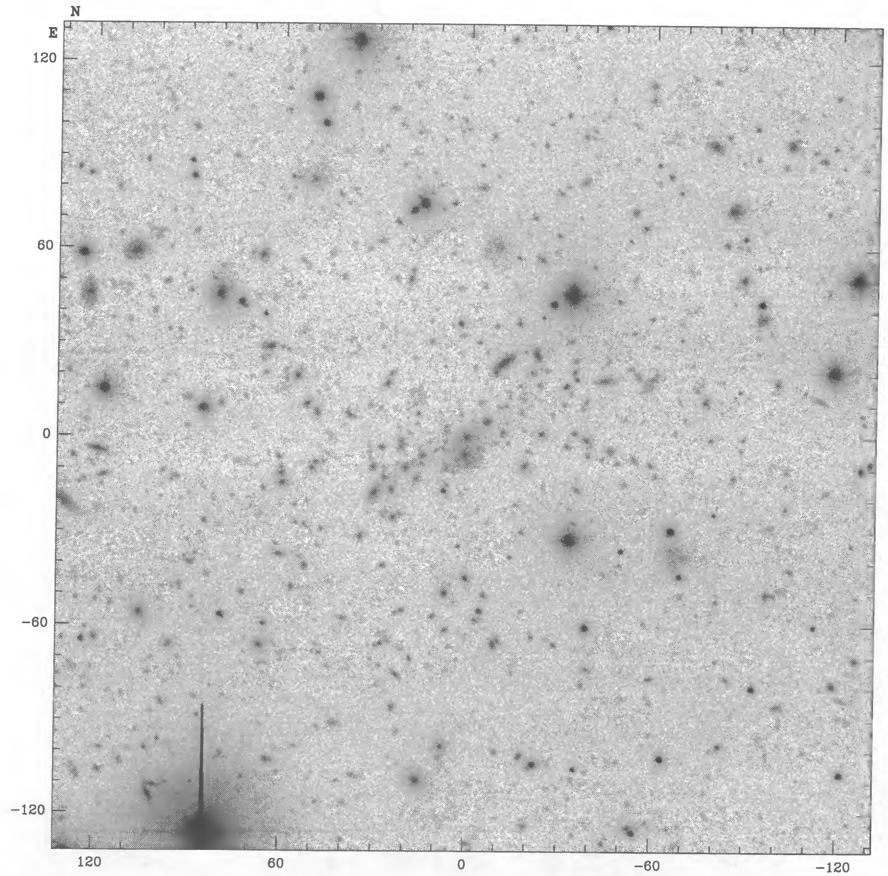

MS 0451.6−0305

Figure 2.9—CCD images of EMSS distant clusters

Redshift:	$z = 0.55$
X-ray luminosity:	$L_{x,44} = 19.97$
Image size/scale:	1200×1200 subarray at $0''.22$/pixel
Field of view:	$4'.4 \times 4'.4$
Scale at cluster redshift:	7.4 kpc/arcsecond
Field at cluster redshift:	1.9 Mpc × 1.9 Mpc
Total exposure time:	7200 s in R
Seeing:	$0''.65$
Notes:	Most X-ray luminous cluster in EMSS.

200 kpc

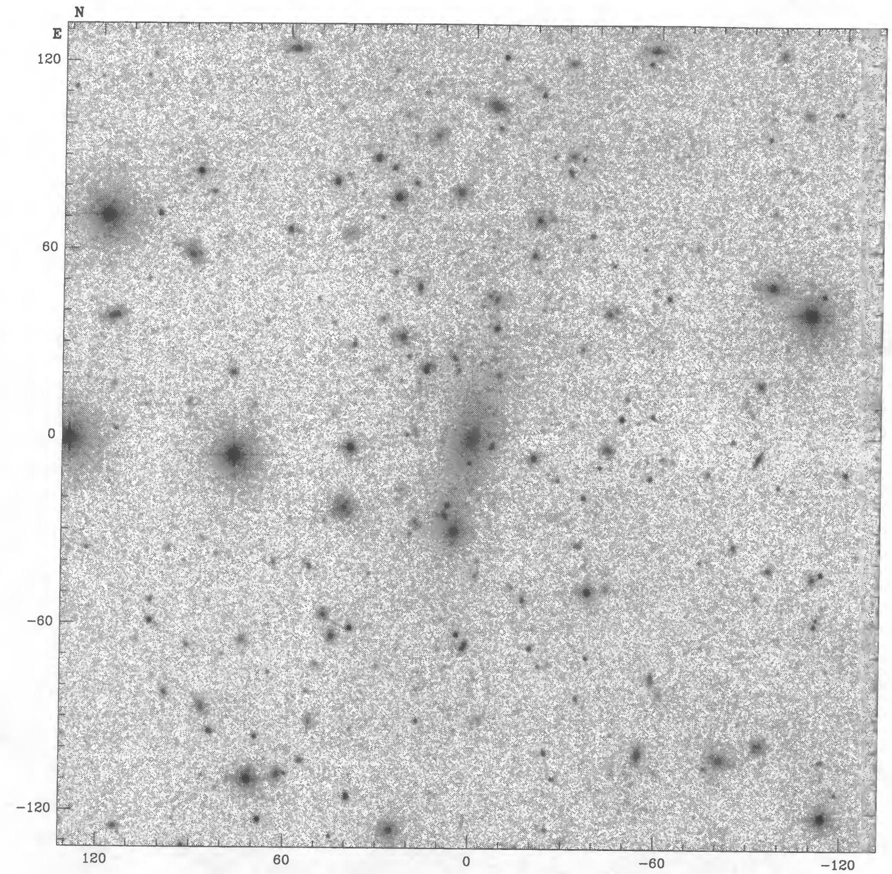

MS 0735.6+7421

Figure 2.10—CCD images of EMSS distant clusters

Redshift:	$z = 0.216$
X-ray luminosity:	$L_{x,44} = 6.12$
Image size/scale:	1200×1200 subarray at $0''.22$/pixel
Field of view:	$4'.4 \times 4'.4$
Scale at cluster redshift:	4.46 kpc/arcsecond
Field at cluster redshift:	1.2 Mpc × 1.2 Mpc
Total exposure time:	1800 s in R
Seeing:	$0''.65$

200 kpc

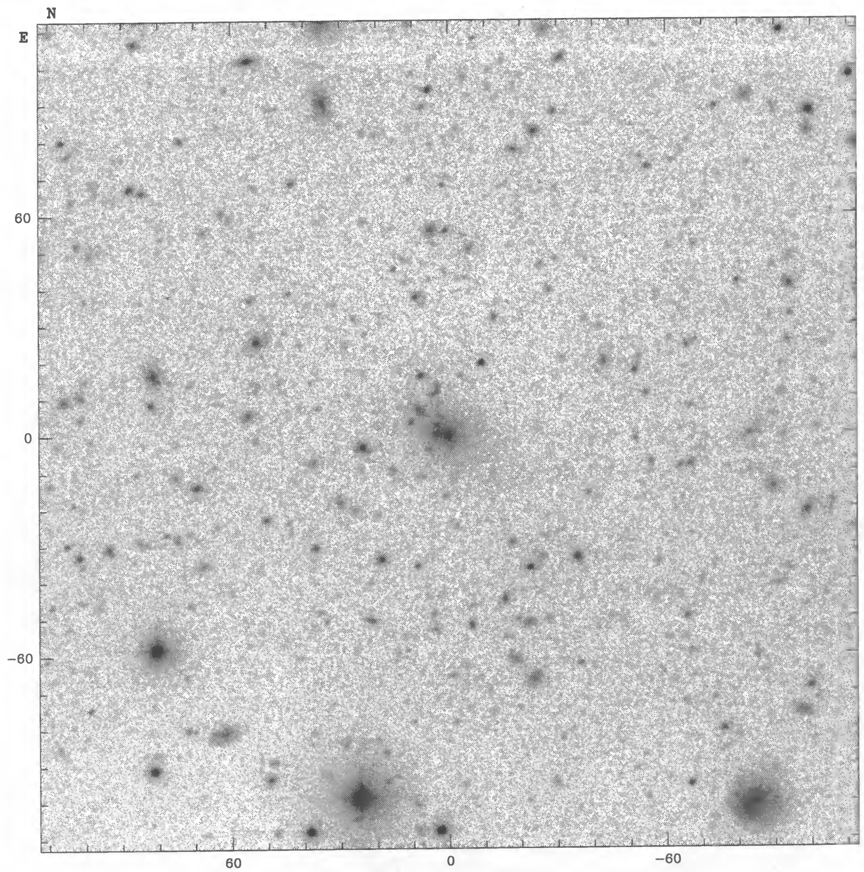

MS 0811.6+6301

Figure 2.11—CCD images of EMSS distant clusters

Redshift:	$z = 0.312$
X-ray luminosity:	$L_{x,44} = 2.10$
Image size/scale:	1024×1024 subarray at $0''.22$/pixel
Field of view:	$3'.8 \times 3'.8$
Scale at cluster redshift:	5.63 kpc/arcsecond
Field at cluster redshift:	1.3 Mpc × 1.3 Mpc
Total exposure time:	3600 s in R
Seeing:	$0''.8$

200 kpc

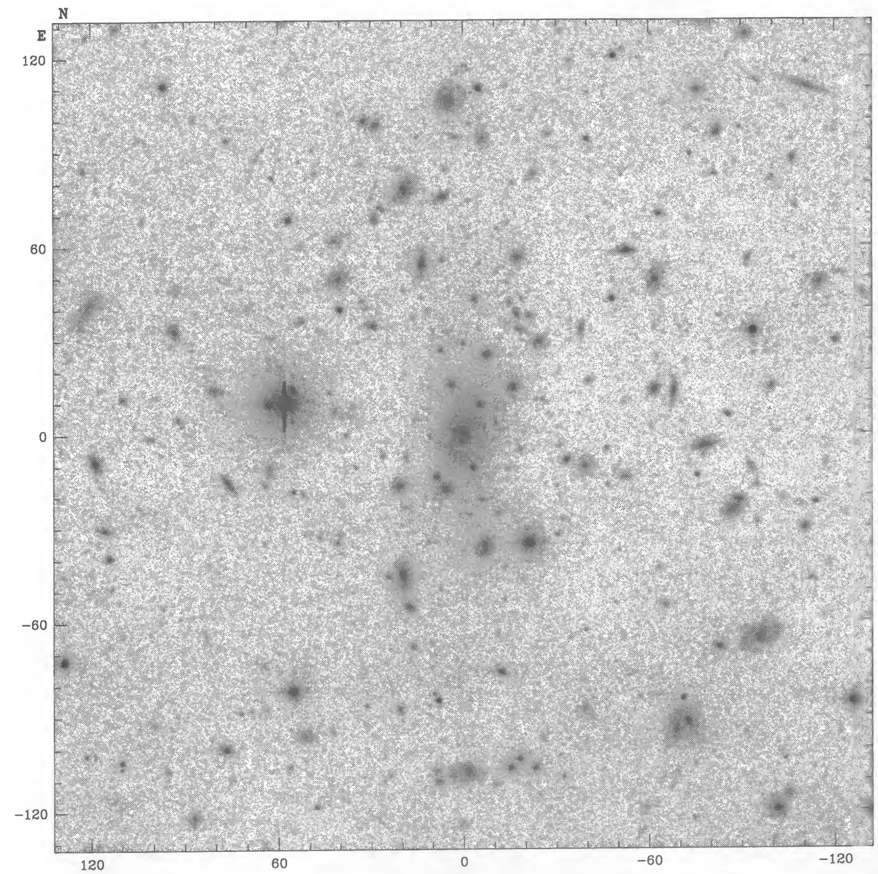

MS 0839.8+2938

Figure 2.12—CCD images of EMSS distant clusters

Redshift:	$z = 0.194$
X-ray luminosity:	$L_{x,44} = 5.35$
Image size/scale:	1200×1200 subarray at $0''.22$/pixel
Field of view:	$4'.4 \times 4'.4$
Scale at cluster redshift:	4.13 kpc/arcsecond
Field at cluster redshift:	1.1 Mpc × 1.1 Mpc
Total exposure time:	900 s in R and 1800 s in B
Seeing:	$0''.7$
Notes:	Many spirals; cooling flow cluster.

200 kpc

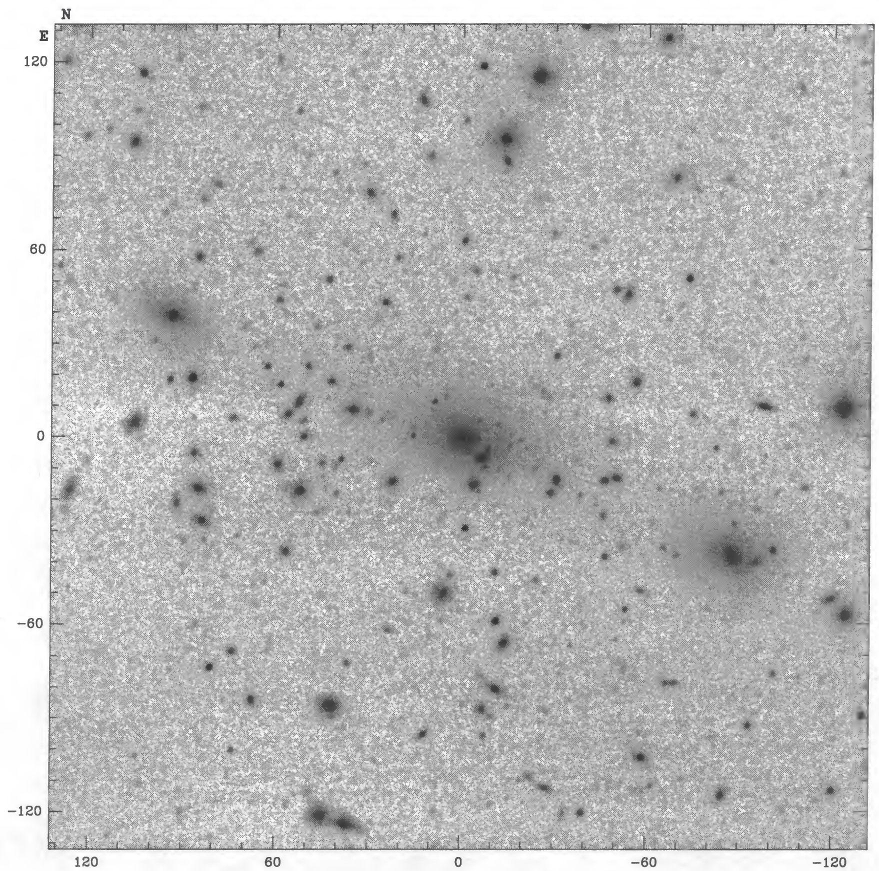

MS 0906.5+1110

Figure 2.13—CCD images of EMSS distant clusters

Redshift:	$z = 0.180$
X-ray luminosity:	$L_{x,44} = 5.77$
Image size/scale:	1200×1200 subarray at $0''.22$/pixel
Field of view:	$4'.4 \times 4'.4$
Scale at cluster redshift:	3.9 kpc/arcsecond
Field at cluster redshift:	1.0 Mpc × 1.0 Mpc
Total exposure time:	2400 s in R
Seeing:	$0''.9$

200 kpc

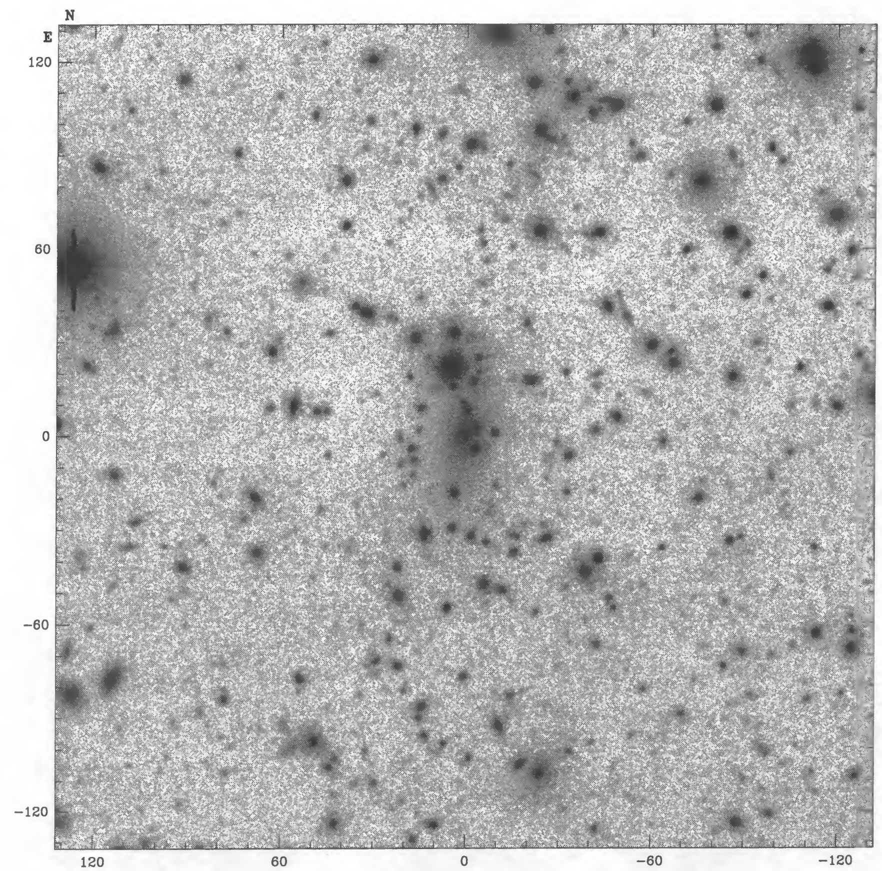

MS 1006.0+1202

Figure 2.14—CCD images of EMSS distant clusters

Redshift:	$z = 0.221$
X-ray luminosity:	$L_{x,44} = 4.82$
Image size/scale:	1200×1200 subarray at $0''.22$/pixel
Field of view:	$4'.4 \times 4'.4$
Scale at cluster redshift:	4.53 kpc/arcsecond
Field at cluster redshift:	1.2 Mpc × 1.2 Mpc
Total exposure time:	2700 s in R
Seeing:	$1''.2$
Notes:	Lensed arcs.

200 kpc

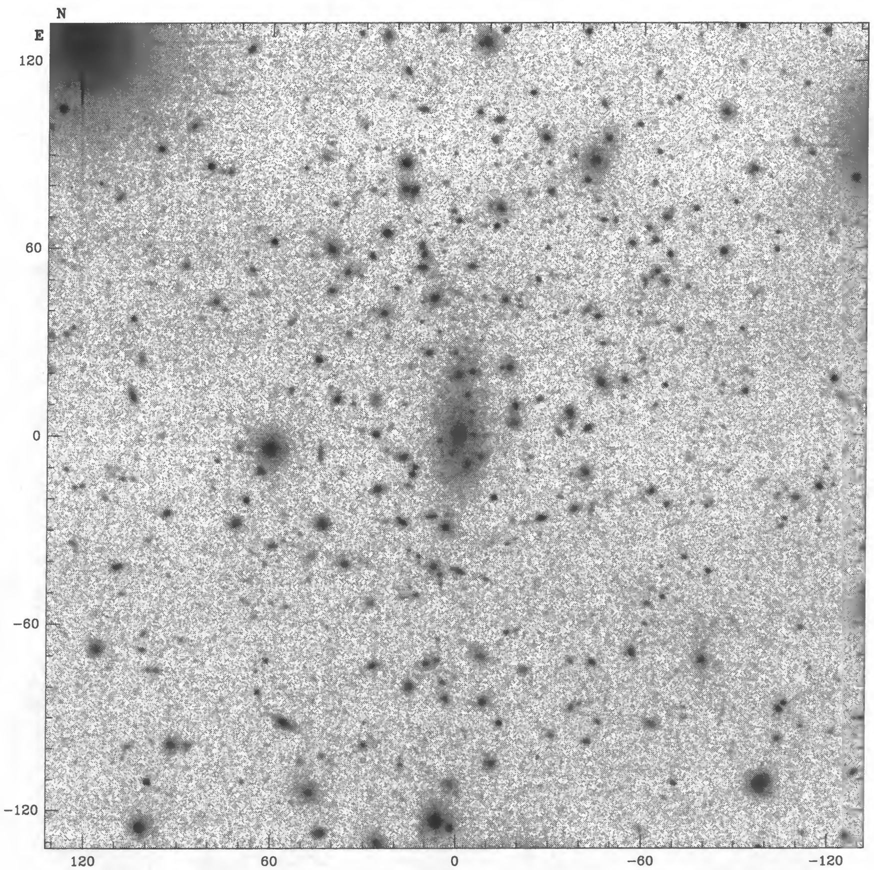

MS 1008.1−1224

Figure 2.15—CCD images of EMSS distant clusters

Redshift:	$z = 0.301$
X-ray luminosity:	$L_{x,44} = 4.49$
Image size/scale:	1200×1200 subarray at $0''.22$/pixel
Field of view:	$4'.4 \times 4'.4$
Scale at cluster redshift:	5.51 kpc/arcsecond
Field at cluster redshift:	1.5 Mpc × 1.5 Mpc
Total exposure time:	2700 s in R
Seeing:	$0''.7$

200 kpc

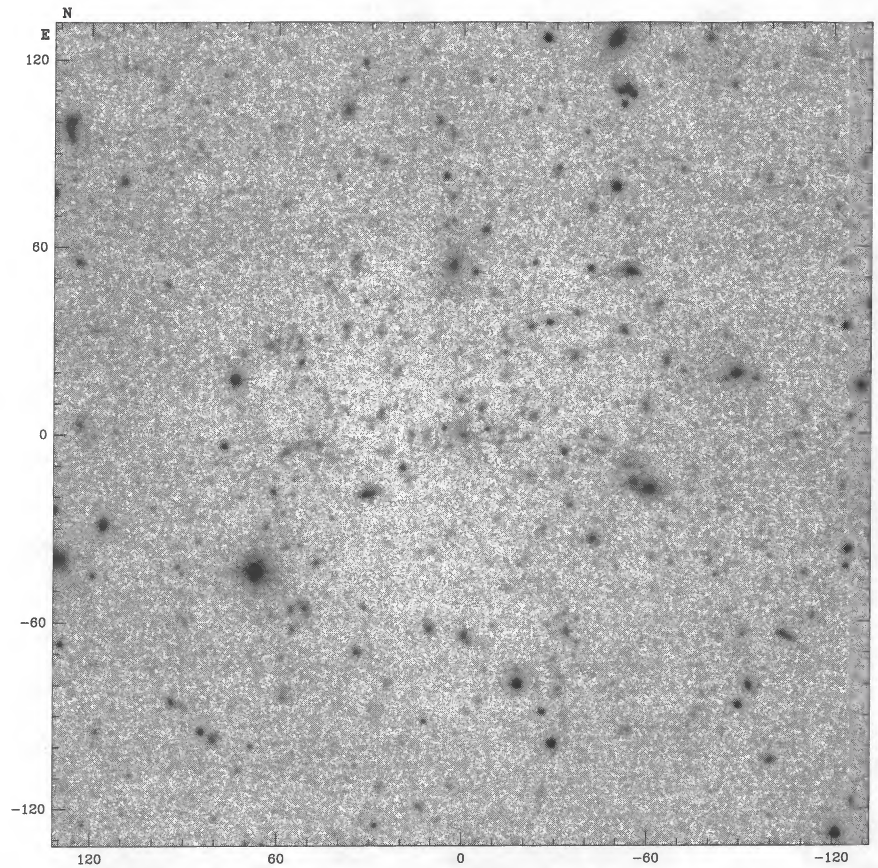

MS 1054.4−0321

Figure 2.16—CCD images of EMSS distant clusters

Redshift:	$z \simeq 0.81$
X-ray luminosity:	$L_{x,44} = 9.02$
Image size/scale:	1200×1200 subarray at $0''.22$/pixel
Field of view:	$4'.4 \times 4'.4$
Scale at cluster redshift:	8.25 kpc/arcsecond
Field at cluster redshift:	2.2 Mpc × 2.2 Mpc
Total exposure time:	7200 s in R
Seeing:	$1''.0$
Notes:	Uncertain redshift; highest-z in EMSS.

200 kpc

1994ApJS...94..583G

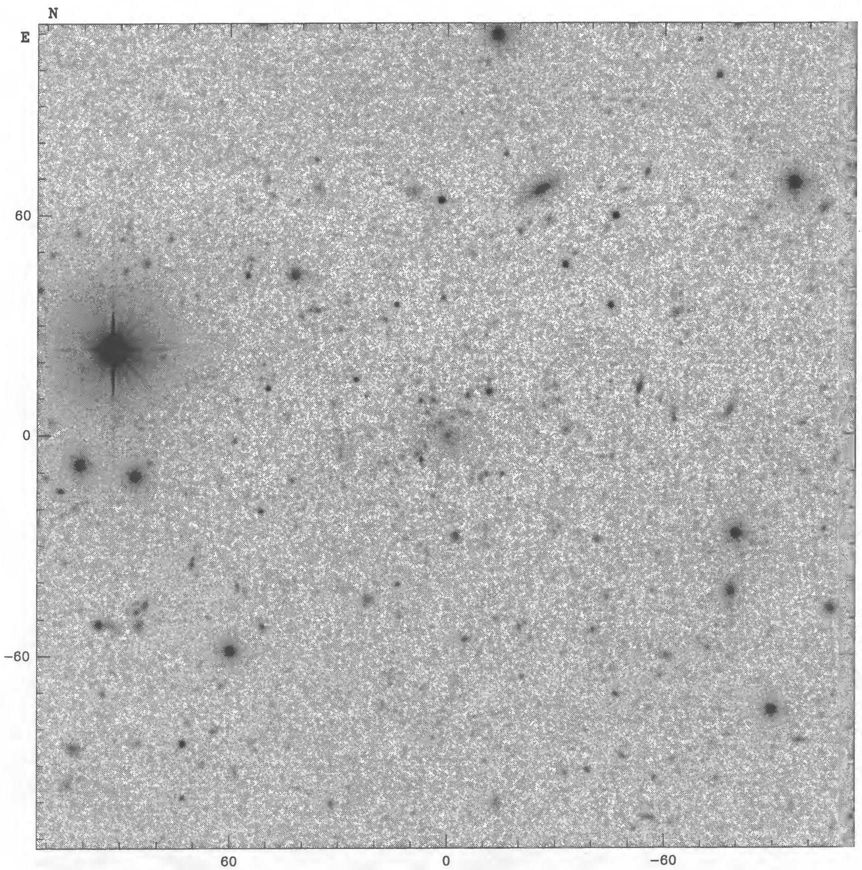

MS 1137.5+6625

Figure 2.17—CCD images of EMSS distant clusters

Redshift:	$z \sim 0.65$ (photometric z)
X-ray luminosity:	$L_{x,44} \sim 5.37$
Image size/scale:	1024 × 1024 subarray at 0″.22/pixel
Field of view:	3′.8 × 3′.8
Scale at cluster redshift:	7.81 kpc/arcsecond
Field at cluster redshift:	1.8 Mpc × 1.8 Mpc
Total exposure time:	3000 s in R
Seeing:	0″.6
Notes:	20′ from 3C263.

200 kpc

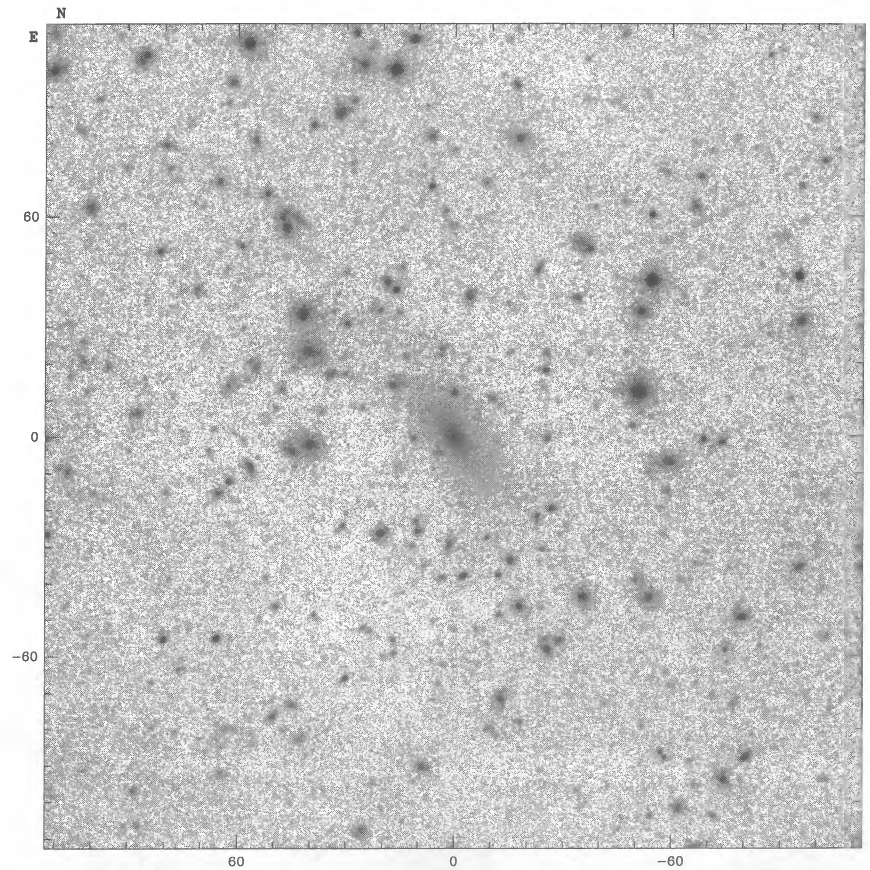

MS 1147.3+1103

Figure 2.18—CCD images of EMSS distant clusters

Redshift:	$z = 0.303$
X-ray luminosity:	$L_{x,44} = 2.30$
Image size/scale:	1024 × 1024 subarray at 0″.22/pixel
Field of view:	3′.8 × 3′.8
Scale at cluster redshift:	5.54 kpc/arcsecond
Field at cluster redshift:	1.2 Mpc × 1.2 Mpc
Total exposure time:	2700 s in R
Seeing:	1″.0

200 kpc

1994ApJS...94..583G

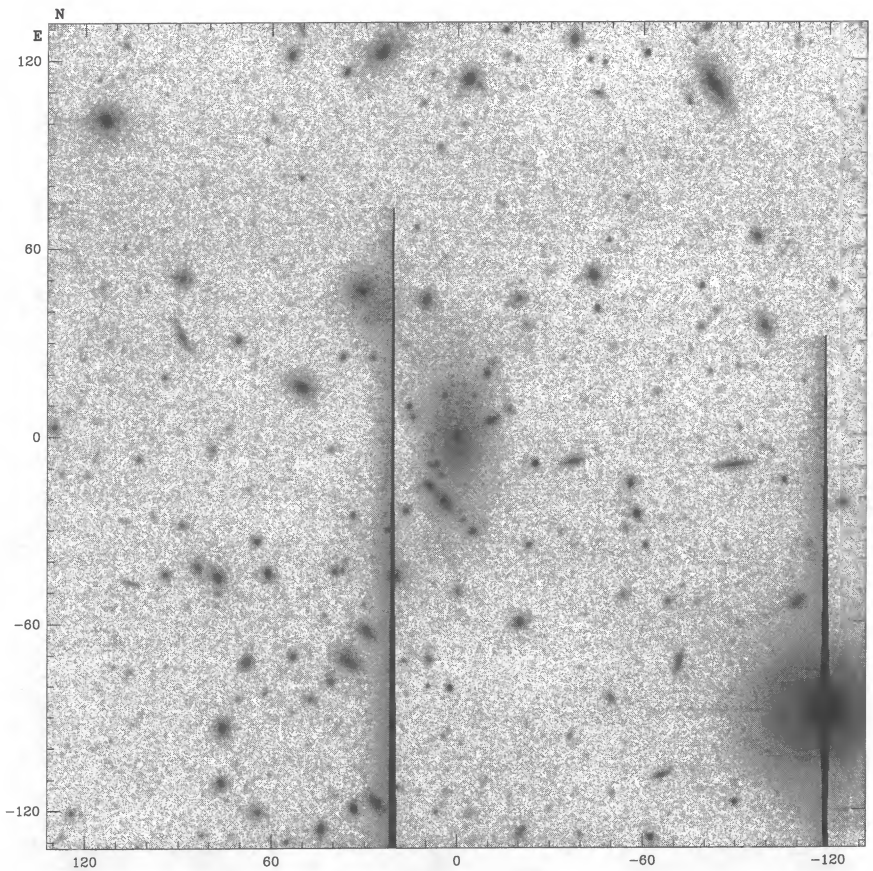

MS 1201.5+2824

Figure 2.19—CCD images of EMSS distant clusters

Redshift:	$z = 0.167$
X-ray luminosity:	$L_{x,44} = 2.02$
Image size/scale:	1200 × 1200 subarray at 0″.22/pixel
Field of view:	4′.4 × 4′.4
Scale at cluster redshift:	3.71 kpc/arcsecond
Field at cluster redshift:	0.98 Mpc × 0.98 Mpc
Total exposure time:	900 s in R
Seeing:	1″.0

200 kpc

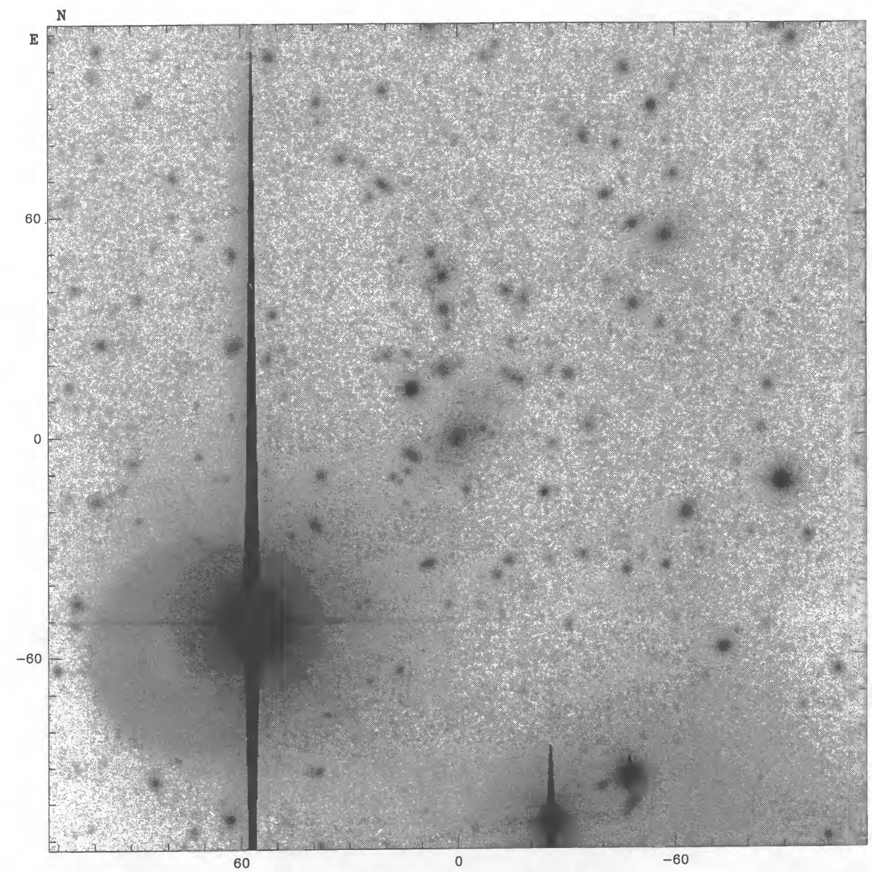

MS 1208.7+3928

Figure 2.20—CCD images of EMSS distant clusters

Redshift:	$z = 0.340$
X-ray luminosity:	$L_{x,44} = 2.03$
Image size/scale:	1024 × 1024 subarray at 0″.22/pixel
Field of view:	3′.8 × 3′.8
Scale at cluster redshift:	5.91 kpc/arcsecond
Field at cluster redshift:	1.3 Mpc × 1.3 Mpc
Total exposure time:	2400 s in R
Seeing:	1″.2

200 kpc

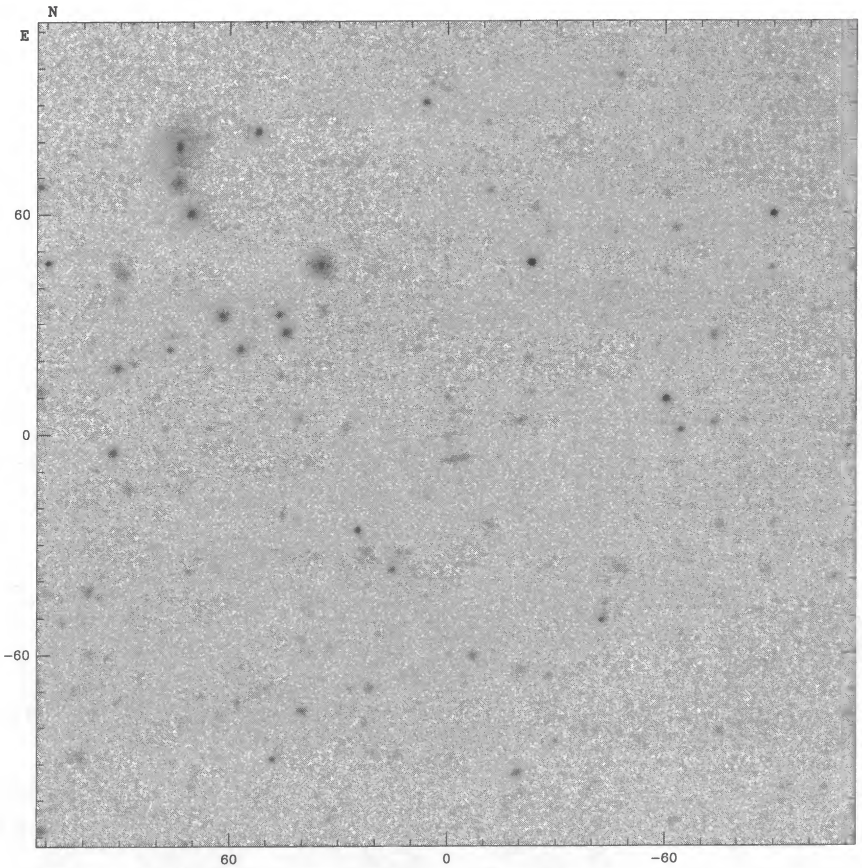

MS 1209.0+3917

Figure 2.21—CCD images of EMSS distant clusters

Redshift:	$z = (.33)$
X-ray luminosity:	$L_{x,44} = (2.49)$
Image size/scale:	1024×1024 subarray at $0''.22$/pixel
Field of view:	$3'.8 \times 3'.8$
Total exposure time:	1800 s in R
Seeing:	$0''.85$
Notes:	Very uncertain ID. Could be a very distant cluster.

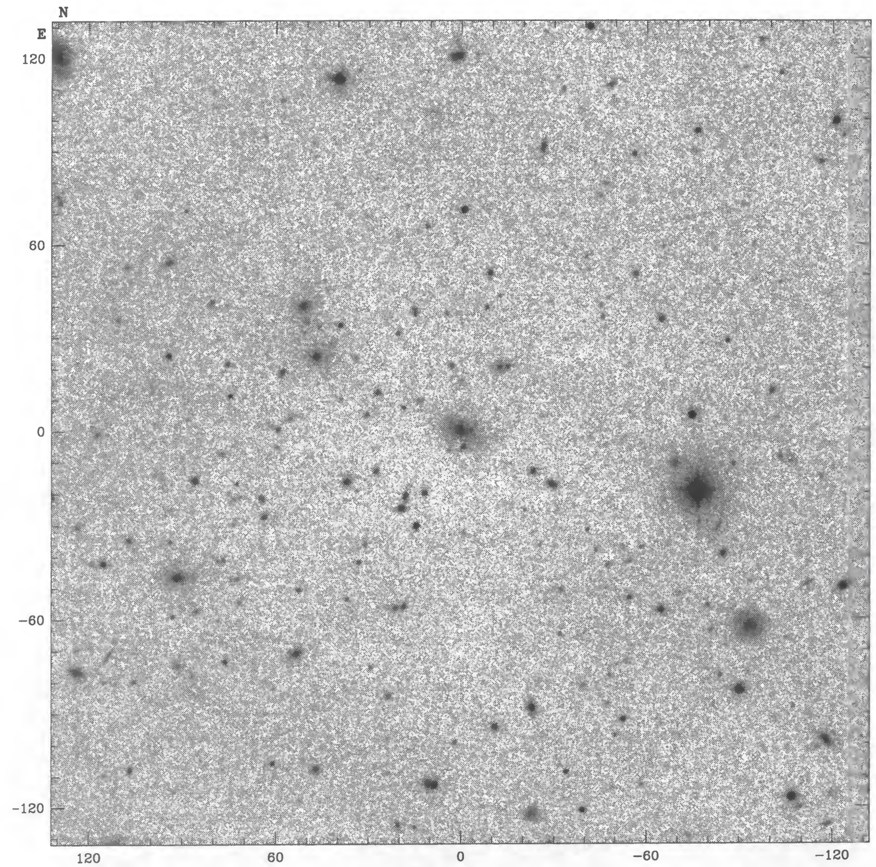

MS 1224.7+2007

Figure 2.22—CCD images of EMSS distant clusters

Redshift:	$z = 0.327$
X-ray luminosity:	$L_{x,44} = 4.61$
Image size/scale:	1200×1200 subarray at $0''.22$/pixel
Field of view:	$4'.4 \times 4'.4$
Scale at cluster redshift:	5.79 kpc/arcsecond
Field at cluster redshift:	1.5 Mpc $\times$ 1.5 Mpc
Total exposure time:	2700 s in R (not photometric)
Seeing:	$0''.9$
Notes:	Image taken through cirrus clouds.

200 kpc

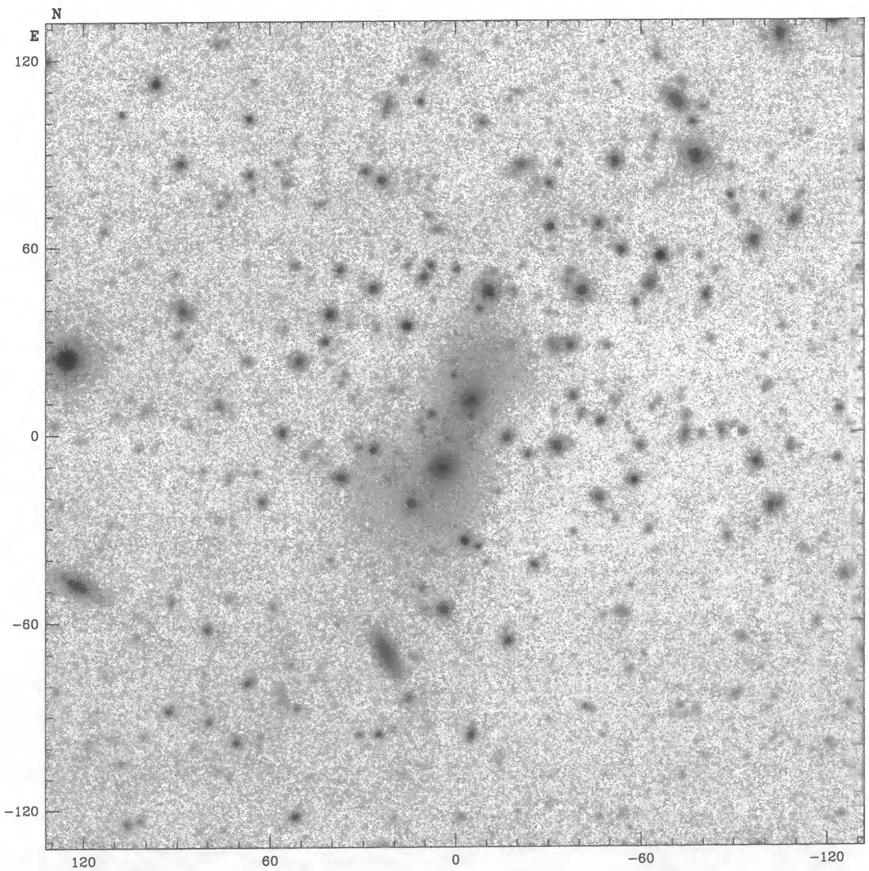

MS 1231.3+1542

Figure 2.23—CCD images of EMSS distant clusters

Redshift:	$z = 0.238$
X-ray luminosity:	$L_{x,44} = 2.88$
Image size/scale:	1200×1200 subarray at $0''.22$/pixel
Field of view:	$4'.4 \times 4'.4$
Scale at cluster redshift:	4.76 kpc/arcsecond
Field at cluster redshift:	1.3 Mpc × 1.3 Mpc
Total exposure time:	2700 s in R
Seeing:	$1''.3$

200 kpc

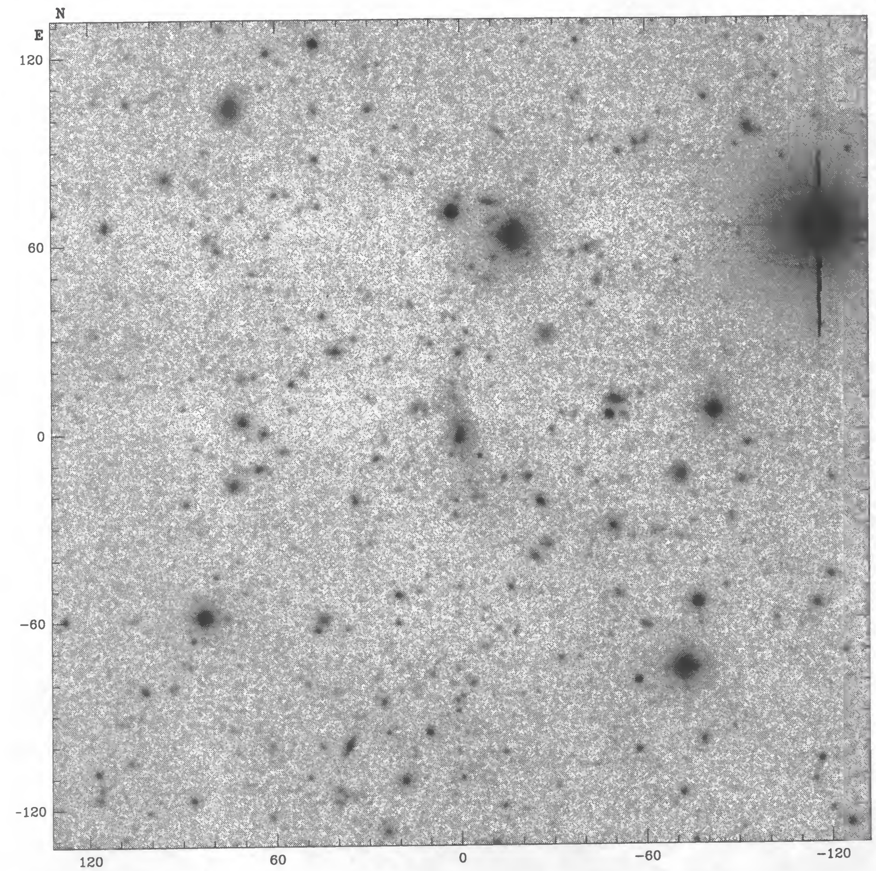

MS 1241.5+1710

Figure 2.24—CCD images of EMSS distant clusters

Redshift:	$z = 0.312$
X-ray luminosity:	$L_{x,44} = 3.41$
Image size/scale:	1200×1200 subarray at $0''.22$/pixel
Field of view:	$4'.4 \times 4'.4$
Scale at cluster redshift:	5.63 kpc/arcsecond
Field at cluster redshift:	1.5 Mpc × 1.5 Mpc
Total exposure time:	2400 s in R
Seeing:	$1''.0$

200 kpc

1994ApJS...94..583G

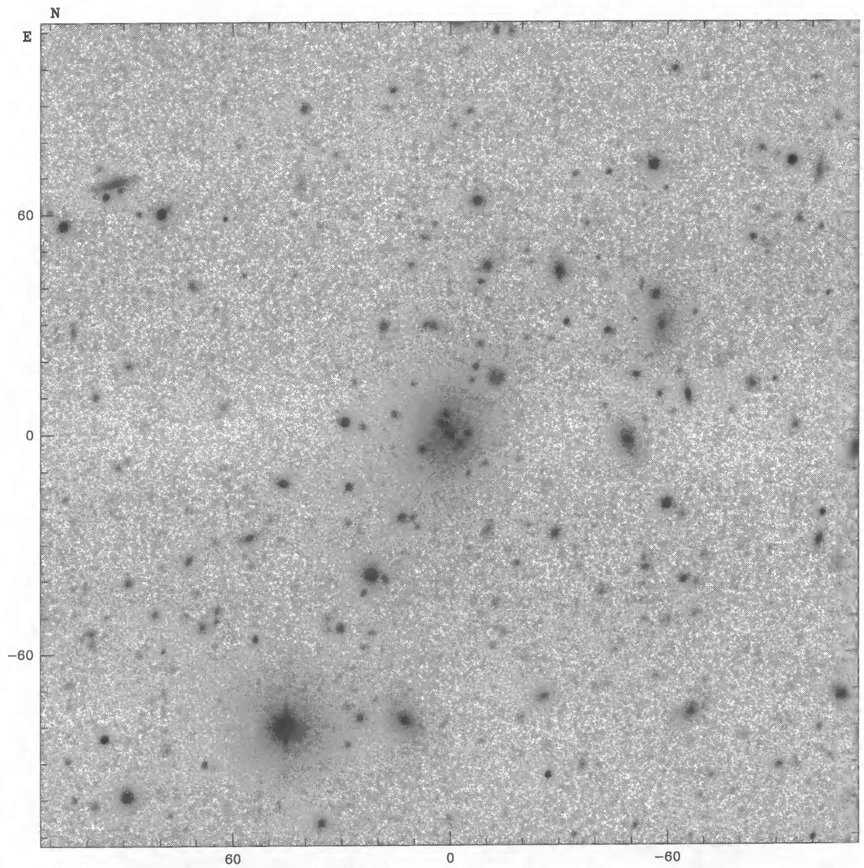

MS 1244.2+7114

Figure 2.25—CCD images of EMSS distant clusters

Redshift: $z = 0.225$
X-ray luminosity: $L_{x,44} = 3.84$
Image size/scale: 1024×1024 subarray at $0''.22$/pixel
Field of view: $3'.8 \times 3'.8$
Scale at cluster redshift: 4.58 kpc/arcsecond
Field at cluster redshift: 1.0 Mpc × 1.0 Mpc
Total exposure time: 2400 s in R
Seeing: $0''.75$
Notes: Merging cD.

200 kpc

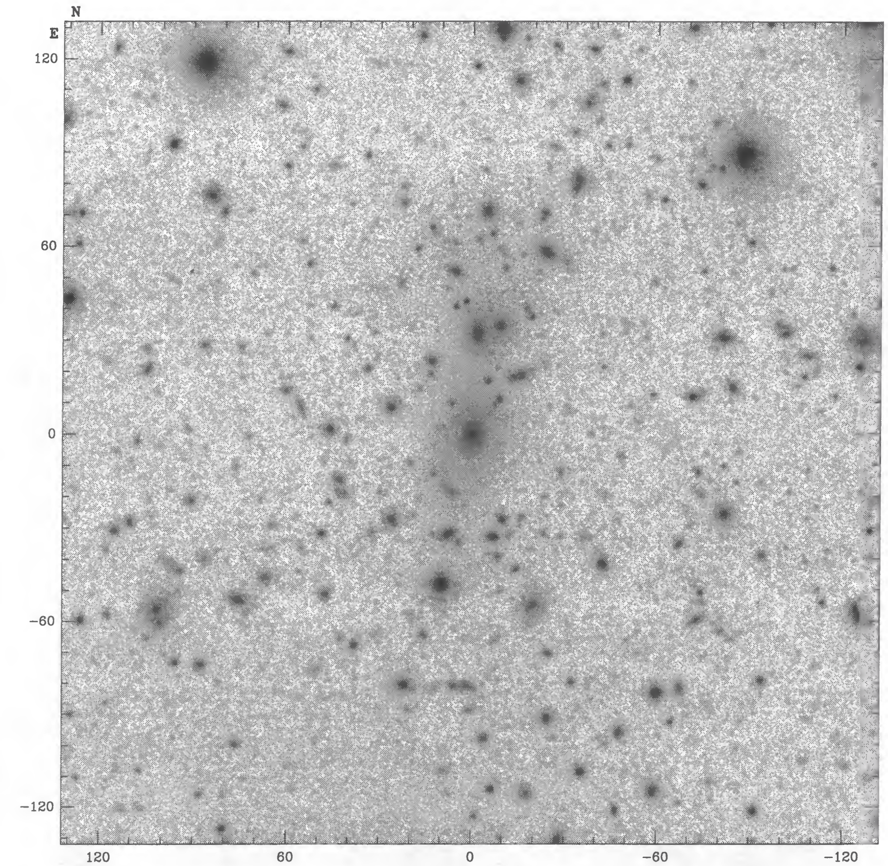

MS 1253.9+0456

Figure 2.26—CCD images of EMSS distant clusters

Redshift: $z = 0.230$
X-ray luminosity: $L_{x,44} = 3.14$
Image size/scale: 1200×1200 subarray at $0''.22$/pixel
Field of view: $4'.4 \times 4'.4$
Scale at cluster redshift: 4.65 kpc/arcsecond
Field at cluster redshift: 1.2 Mpc × 1.2 Mpc
Total exposure time: 3000 s in R
Seeing: $0''.8$

200 kpc

1994ApJS...94..583G

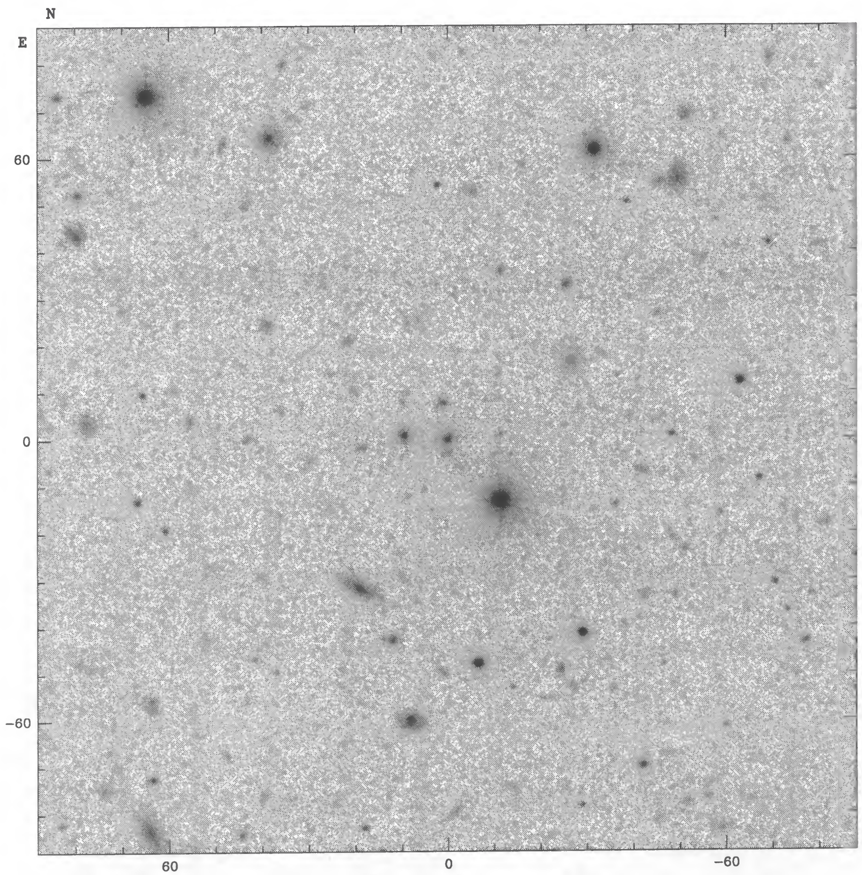

MS 1333.3+1725

Figure 2.27—CCD images of EMSS distant clusters

Redshift:	$z = 0.46$
X-ray luminosity:	$L_{x,44} = 5.40$
Image size/scale:	800×800 subarray at $0''.22$/pixel
Field of view:	$2'.9 \times 2'.9$
Scale at redshift:	6.87 kpc/arcsecond
Field at redshift:	1.2 Mpc $\times$ 1.2 Mpc
Total exposure time:	2400 s in R
Seeing:	$0''.65$
Notes:	Uncertain ID.

200 kpc

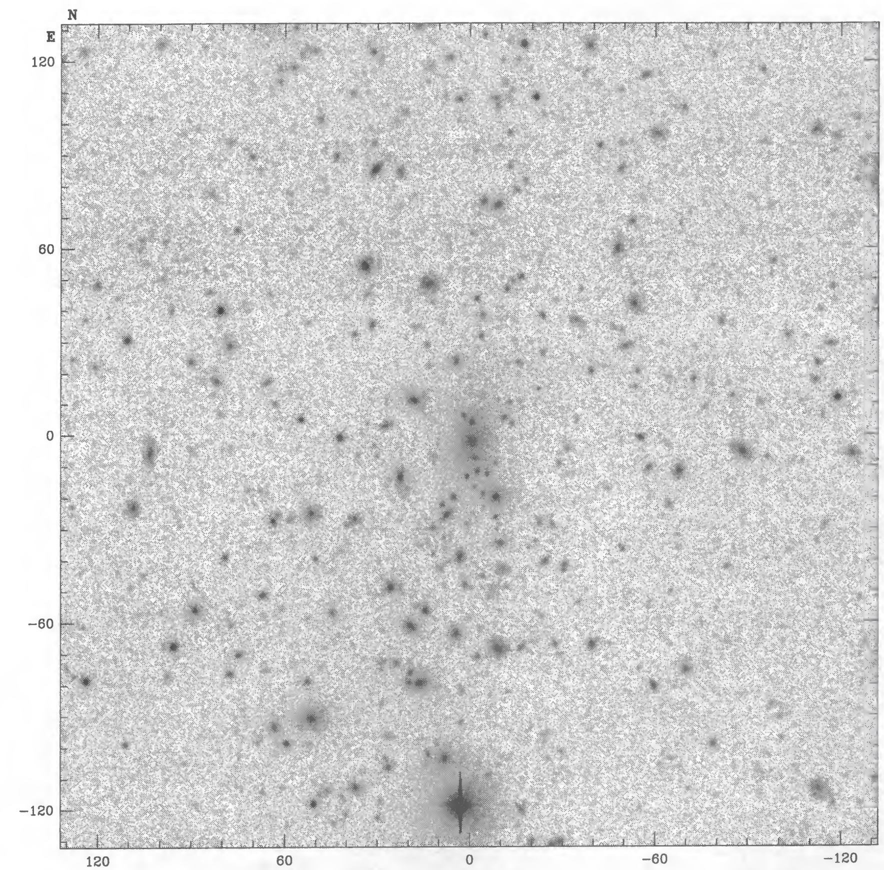

MS 1358.4+6245

Figure 2.28—CCD images of EMSS distant clusters

Redshift:	$z = 0.327$
X-ray luminosity:	$L_{x,44} = 10.62$
Image size/scale:	1200×1200 subarray at $0''.22$/pixel
Field of view:	$4'.4 \times 4'.4$
Scale at cluster redshift:	5.80 kpc/arcsecond
Field at cluster redshift:	1.5 Mpc $\times$ 1.5 Mpc
Total exposure time:	1800 s in R
Seeing:	$0''.9$

200 kpc

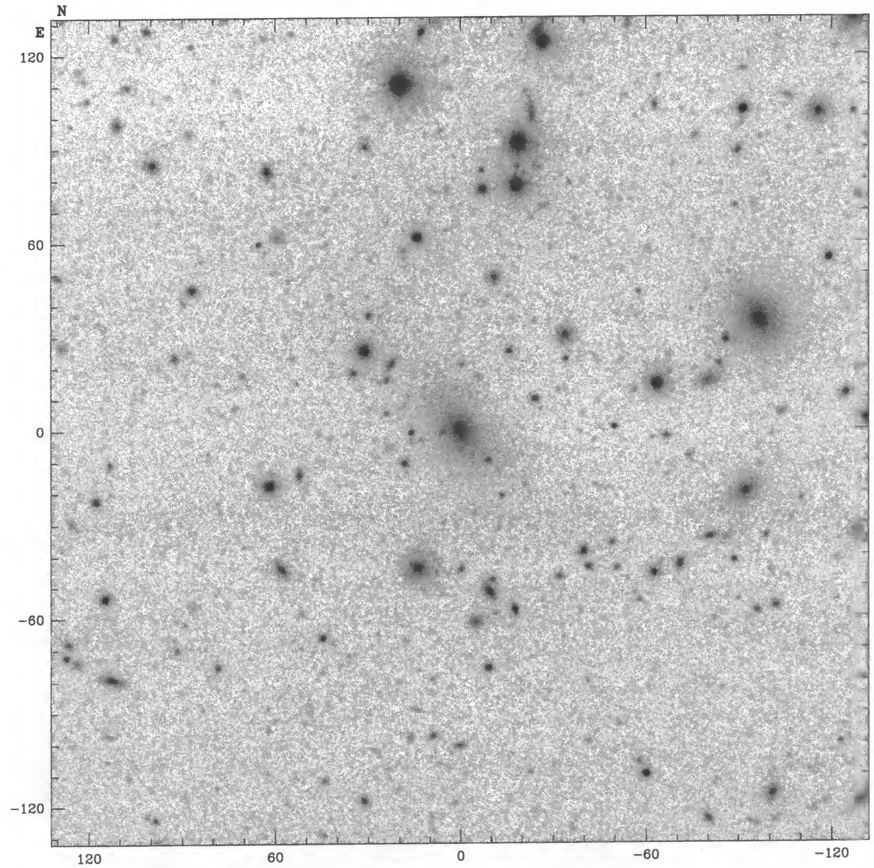

MS 1455.0+2232

Figure 2.30—CCD images of EMSS distant clusters

Redshift:	$z = 0.259$
X-ray luminosity:	$L_{x,44} = 16.03$
Image size/scale:	1200×1200 subarray at $0''.22$/pixel
Field of view:	$4'.4 \times 4'.4$
Scale at cluster redshift:	5.03 kpc/arcsecond
Field at cluster redshift:	1.3 Mpc $\times$ 1.3 Mpc
Total exposure time:	1800 s in R
Seeing:	$0''.8$
Notes:	Faint, lensed arc NE of cD galaxy.

200 kpc

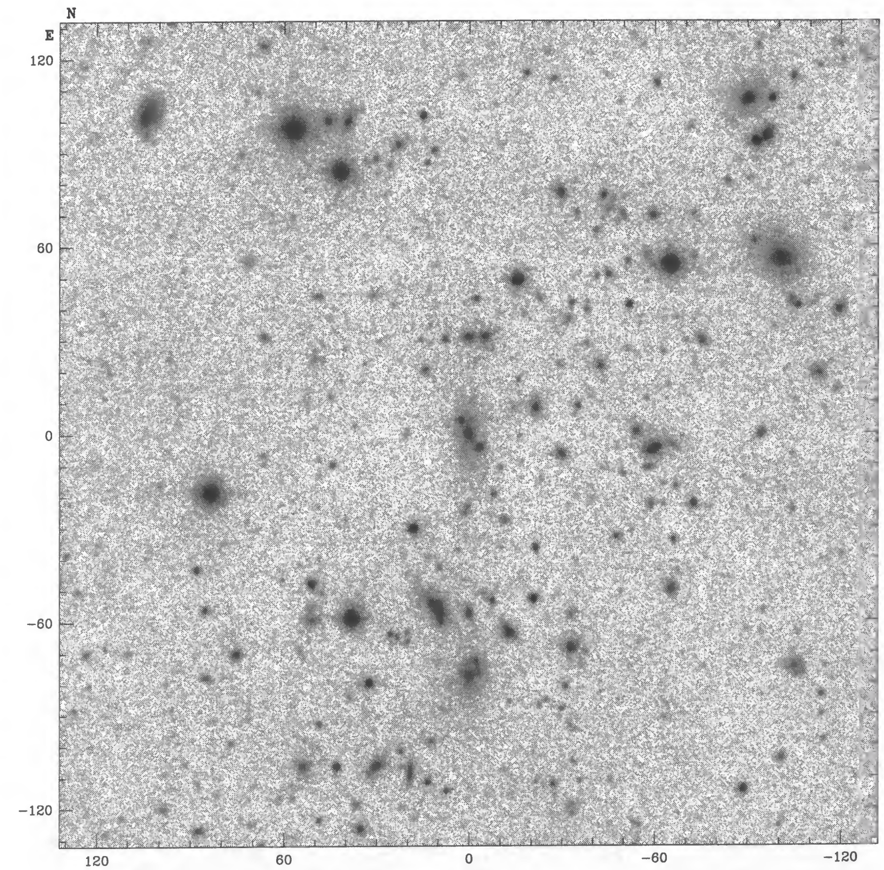

MS 1426.4+0158

Figure 2.29—CCD images of EMSS distant clusters

Redshift:	$z = 0.320$
X-ray luminosity:	$L_{x,44} = 3.71$
Image size/scale:	1200×1200 subarray at $0''.22$/pixel
Field of view:	$4'.4 \times 4'.4$
Scale at cluster redshift:	5.71 kpc/arcsecond
Field at cluster redshift:	1.5 Mpc $\times$ 1.5 Mpc
Total exposure time:	900 s in R
Seeing:	$1''.1$

200 kpc

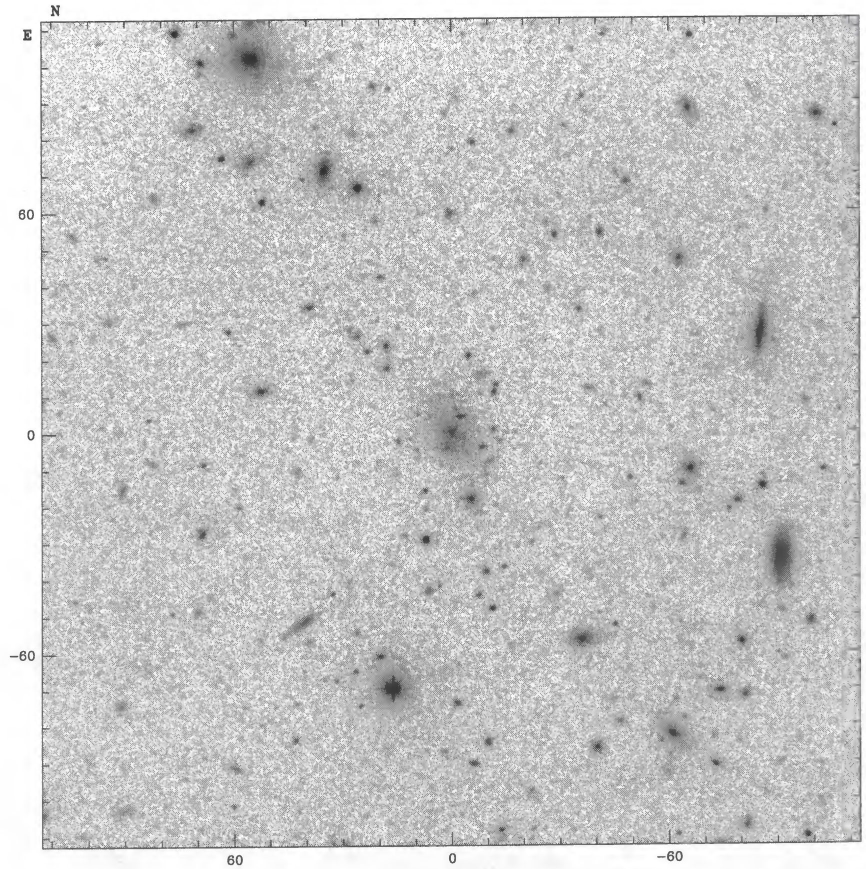

MS 1512.4+3647

Figure 2.31—CCD images of EMSS distant clusters

Redshift:	$z = 0.372$
X-ray luminosity:	$L_{x,44} = 4.81$
Image size/scale:	1024×1024 subarray at $0''.22$/pixel
Field of view:	$3'.8 \times 3'.8$
Scale at cluster redshift:	6.20 kpc/arcsecond
Field at cluster redshift:	1.4 Mpc × 1.4 Mpc
Total exposure time:	1800 s in R
Seeing:	$0''.6$
Notes:	Bright, blue, elongated object in NW of core.

200 kpc

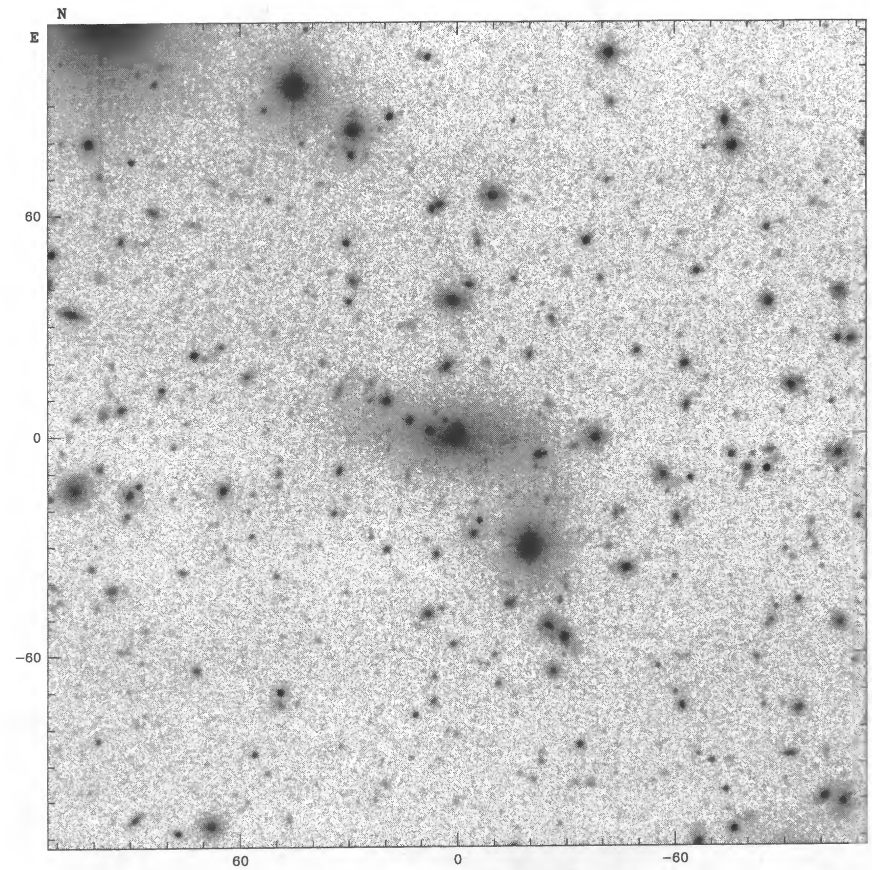

MS 1546.8+1132

Figure 2.32—CCD images of EMSS distant clusters

Redshift:	$z = 0.226$
X-ray luminosity:	$L_{x,44} = 2.94$
Image size/scale:	1024×1024 subarray at $0''.22$/pixel
Field of view:	$3'.8 \times 3'.8$
Scale at cluster redshift:	4.59 kpc/arcsecond
Field at cluster redshift:	1.0 Mpc × 1.0 Mpc
Total exposure time:	3000 s in R
Seeing:	$0''.8$

200 kpc

1994ApJS...94..583G

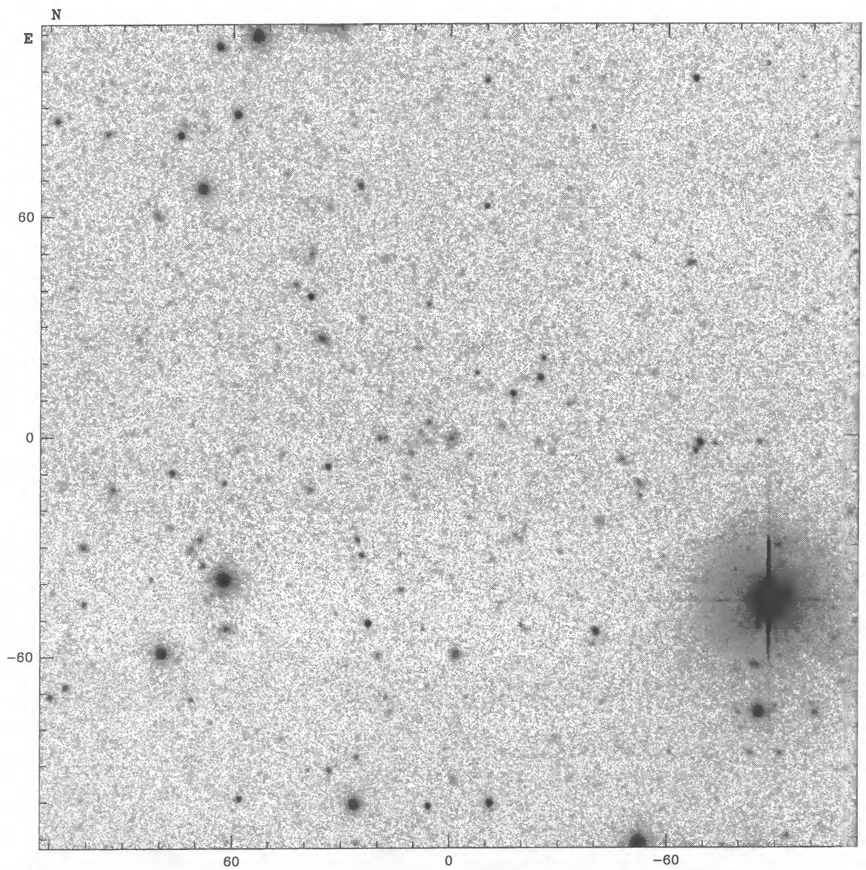

MS 1610.4+6616

Figure 2.33—CCD images of EMSS distant clusters

Redshift:	$z \simeq 0.55$
X-ray luminosity:	$L_{x,44} = 4.70$
Image size/scale:	1024×1024 subarray at $0''.22$/pixel
Field of view:	$3'.8 \times 3'.8$
Scale at cluster redshift:	7.38 kpc/arcsecond
Field at cluster redshift:	1.66 Mpc $\times$ 1.66 Mpc
Total exposure time:	1800 s in R
Seeing:	$0''.8$
Notes:	Preliminary z; previously unidentified.

200 kpc

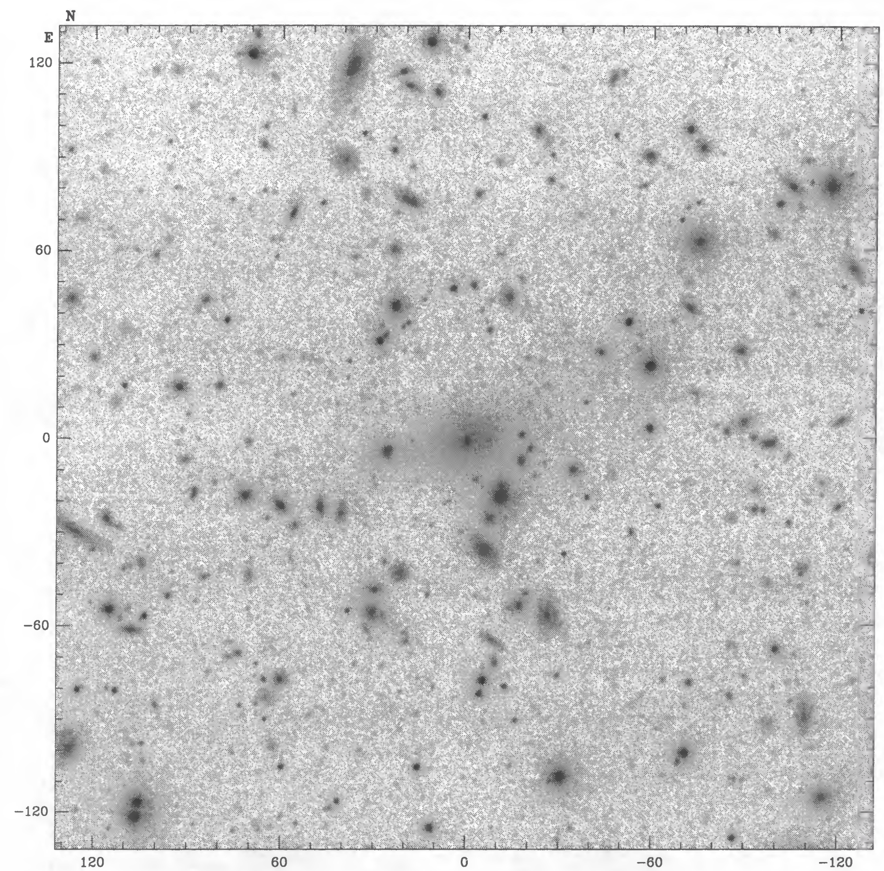

MS 1618.9+2552

Figure 2.34—CCD images of EMSS distant clusters

Redshift:	$z = 0.161$
X-ray luminosity:	$L_{x,44} = 2.24$
Image size/scale:	1200×1200 subarray at $0''.22$/pixel
Field of view:	$4'.4 \times 4'.4$
Scale at cluster redshift:	3.60 kpc/arcsecond
Field at cluster redshift:	0.95 Mpc $\times$ 0.95 Mpc
Total exposure time:	2400 s in R
Seeing:	$0''.8$

200 kpc

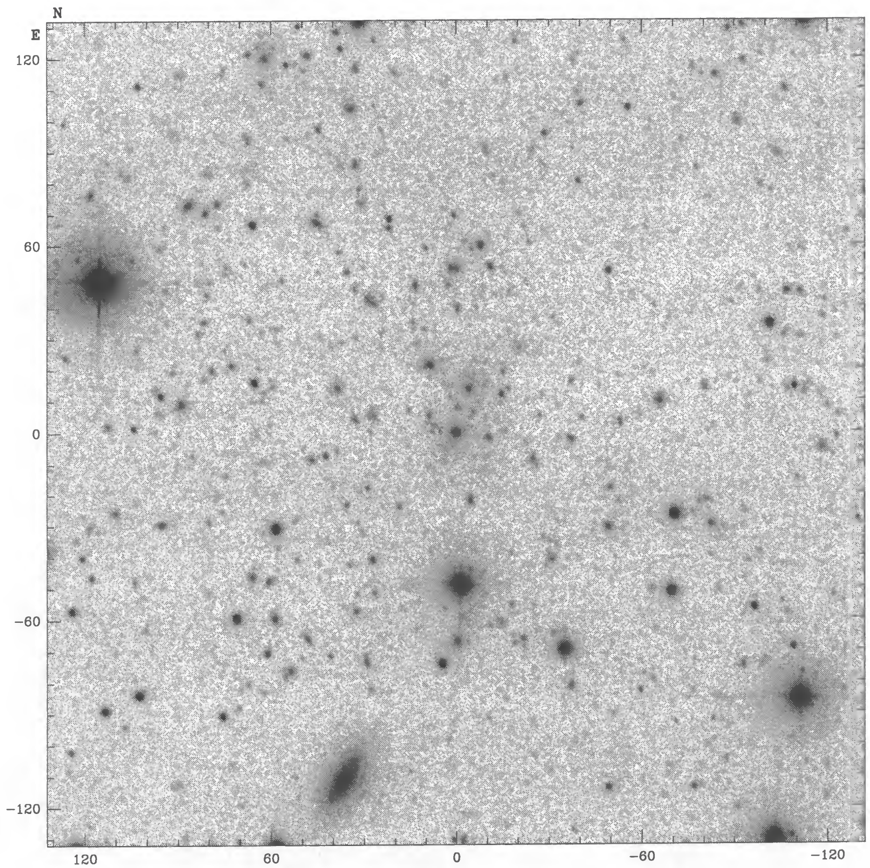

MS 1621.5+2640

Figure 2.35—CCD images of EMSS distant clusters

Redshift:	$z = 0.426$
X-ray luminosity:	$L_{x,44} = 4.55$
Image size/scale:	1200×1200 subarray at $0''.22$/pixel
Field of view:	$4'.4 \times 4'.4$
Scale at cluster redshift:	6.63 kpc/arcsecond
Field at cluster redshift:	1.8 Mpc $\times$ 1.8 Mpc
Total exposure time:	1800 s in R
Seeing:	$1''.1$
Notes:	Lensed arc centered on radio galaxy.

200 kpc

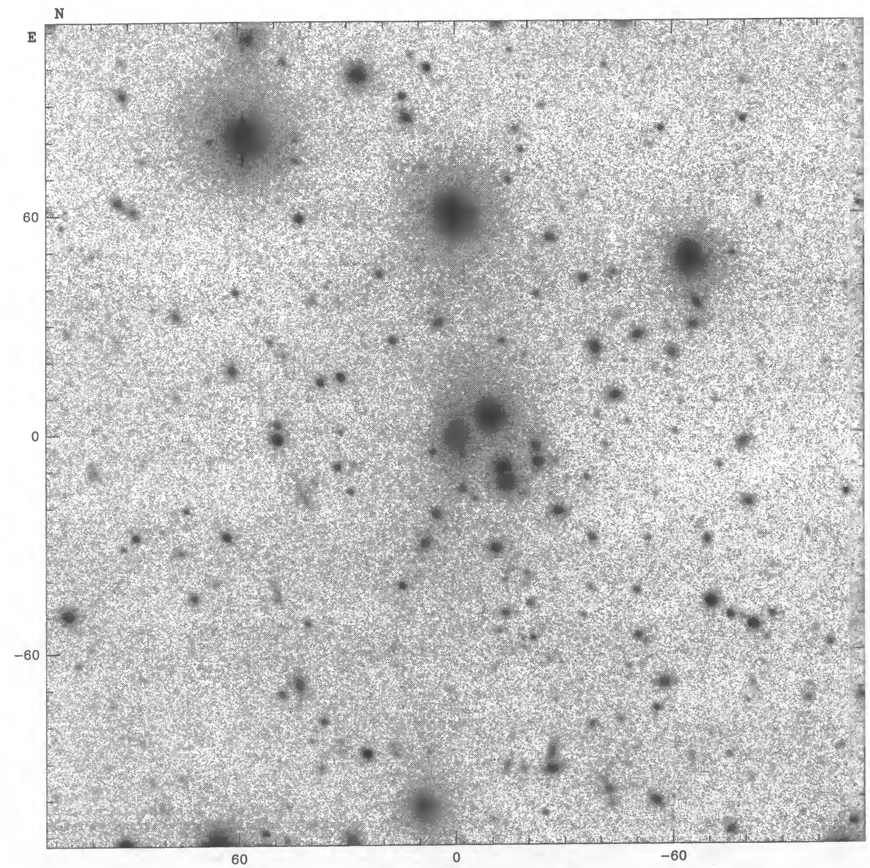

MS 1910.5+6736

Figure 2.36—CCD images of EMSS distant clusters

Redshift:	$z = 0.246$
X-ray luminosity:	$L_{x,44} = 4.39$
Image size/scale:	1024×1024 subarray at $0''.22$/pixel
Field of view:	$3'.8 \times 3'.8$
Scale at cluster redshift:	4.86 kpc/arcsecond
Field at cluster redshift:	1.1 Mpc $\times$ 1.1 Mpc
Total exposure time:	1800 s in R
Seeing:	$1''.0$
Notes:	Possible lensed arc to SE.

200 kpc

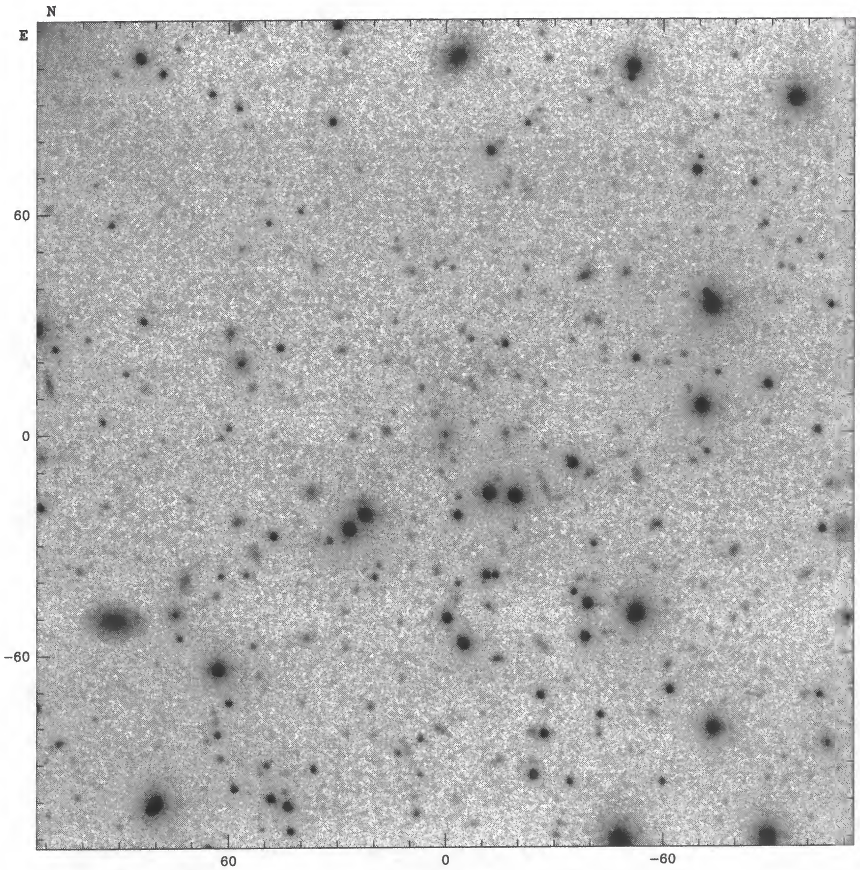

MS 2053.7−0449

Figure 2.37—CCD images of EMSS distant clusters

Redshift:	$z = 0.583$
X-ray luminosity:	$L_{x,44} = 5.77$
Image size/scale:	1024×1024 subarray at $0''.22$/pixel
Field of view:	$3'.8 \times 3'.8$
Scale at cluster redshift:	7.55 kpc/arcsecond
Field at cluster redshift:	1.7 Mpc × 1.7 Mpc
Total exposure time:	6000 s in R
Seeing:	$0''.8$
Notes:	Lensed arcs to NW.

200 kpc

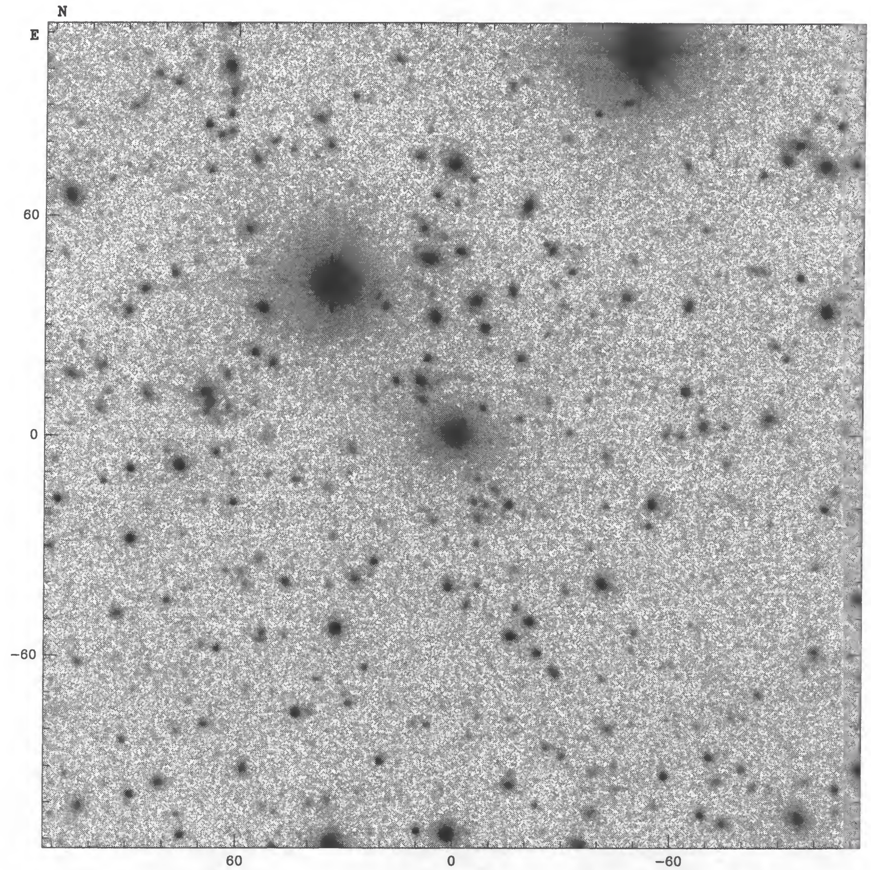

MS 2137.3−2353

Figure 2.38—CCD images of EMSS distant clusters

Redshift:	$z = 0.313$
X-ray luminosity:	$L_{x,44} = 15.62$
Image size/scale:	1024×1024 subarray at $0''.22$/pixel
Field of view:	$3'.8 \times 3'.8$
Scale at cluster redshift:	5.64 kpc/arcsecond
Field at cluster redshift:	1.3 Mpc × 1.3 Mpc
Total exposure time:	3600 s in R
Seeing:	$1''.0$
Notes:	Lensed arcs.

200 kpc

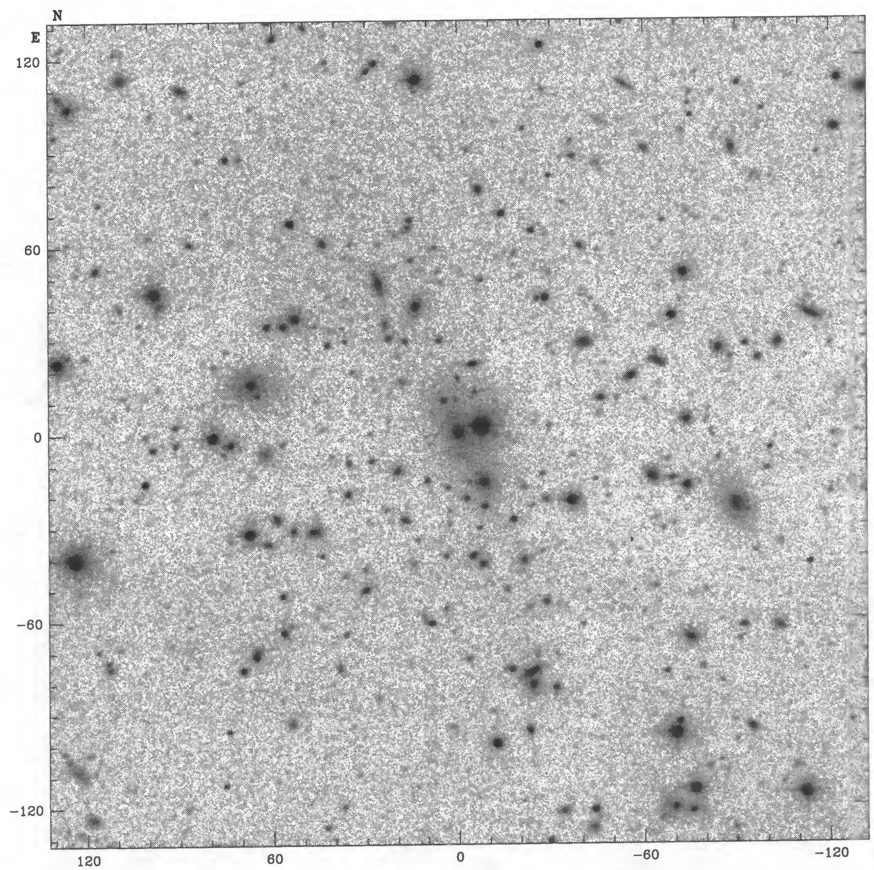

MS 2255.7+2039

Figure 2.39—CCD images of EMSS distant clusters

Redshift:	$z = 0.288$
X-ray luminosity:	$L_{x,44} = 2.04$
Image size/scale:	1200 × 1200 subarray at 0″.22/pixel
Field of view:	4′.4 × 4′.4
Scale at cluster redshift:	5.37 kpc/arcsecond
Field at cluster redshift:	1.4 Mpc × 1.4 Mpc
Total exposure time:	3000 s in R
Seeing:	0″.8

200 kpc

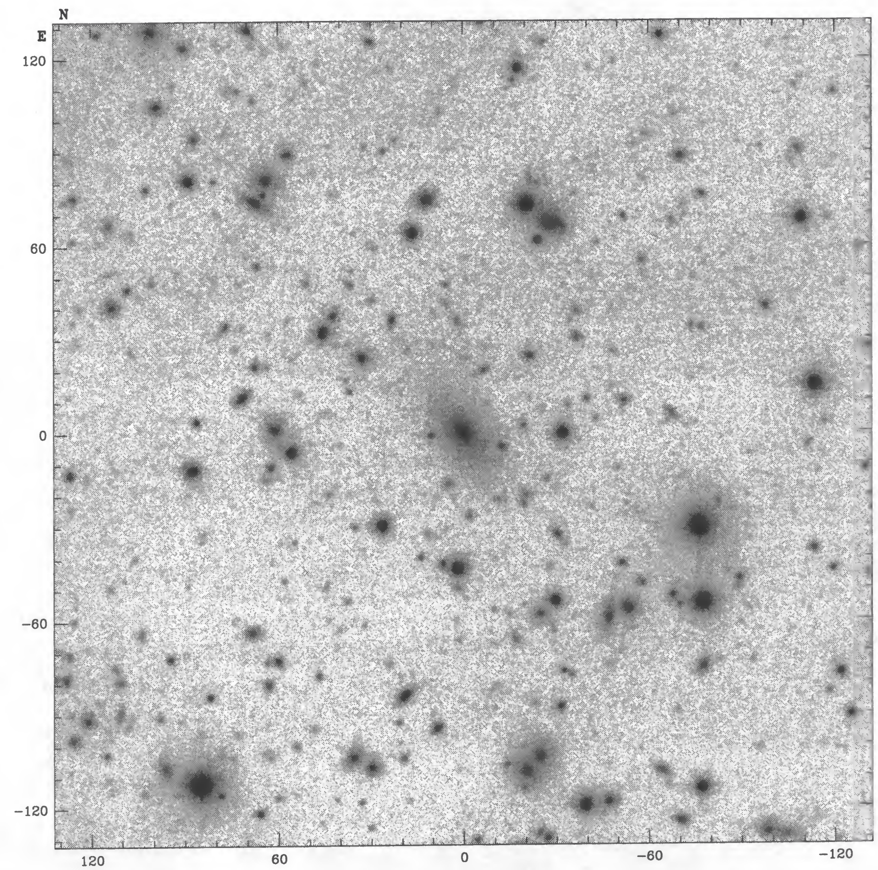

MS 2301.3+1506

Figure 2.40—CCD images of EMSS distant clusters

Redshift:	$z = 0.247$
X-ray luminosity:	$L_{x,44} = 3.29$
Image size/scale:	1200 × 1200 subarray at 0″.22/pixel
Field of view:	4′.4 × 4′.4
Scale at cluster redshift:	4.88 kpc/arcsecond
Field at cluster redshift:	1.3 Mpc × 1.3 Mpc
Total exposure time:	6000 s in R
Seeing:	1″.0

200 kpc

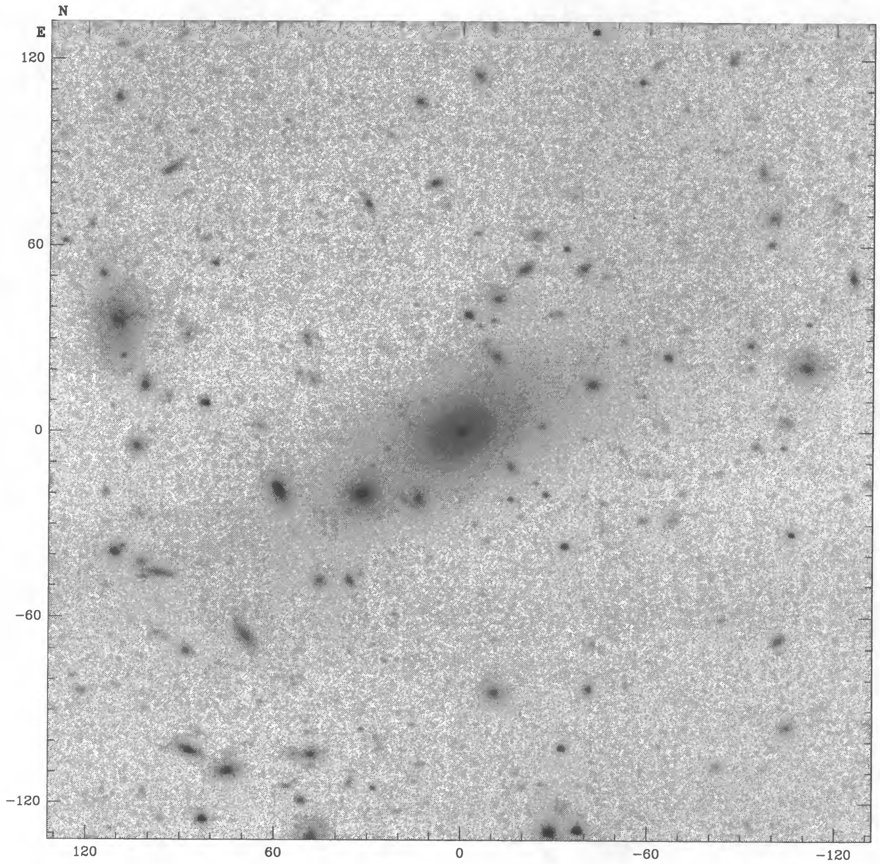

MS 2318.7−2328

Figure 2.41—CCD images of EMSS distant clusters

Redshift:	$z = 0.187$
X-ray luminosity:	$L_{x,44} = 6.84$
Image size/scale:	1200 × 1200 subarray at 0″.22/pixel
Field of view:	4′.4 × 4′.4
Scale at cluster redshift:	4.03 kpc/arcsecond
Field at cluster redshift:	1.1 Mpc × 1.1 Mpc
Total exposure time:	1800s in R
Seeing:	1″.0

200 kpc

other hand, there are two objects, MS 1209.0+3917 and MS 1333.3+1725, whose identification with a cluster is questionable. The first source was identified as a "cooling flow galaxy" in Stocke et al. (1991) and is here presented as a cluster due to the presence of a few galaxies around it. Both clusters look like very poor systems (unless they are very distant ones). We would like to stress that these two identifications are tentative and the need for more spectroscopy or deeper imaging is in order.

TABLE 3

UNIDENTIFIED SOURCES

(1) EMSS Name	(2) $F_x^{\rm Det} \times 10^{-13}$
MS 0235.6+1631	1.74
MS 0354.2−3658	3.30
MS 0501.0−2237	3.19
MS 1237.9−2927	4.86
MS 1411.0−0310	1.83
MS 2136.1−1509	2.50
MS 2144.2+0358	1.74
MS 2223.8−0503	1.59
MS 2225.7−2100	1.33

The high quality of the CCD images will allow us to study the brightest cluster galaxies. In several cases (MS 0440.5+0204, MS 1244.2+7114, and MS 2124.7−2206) the central galaxy is composed of multiple nuclei embedded in a common envelope. In some cases it consists of double nuclei (e.g., MS 0906.5+1110 and MS 1910.5+6736) or triple nuclei (e.g., MS 0353.6−3642 and MS 1426.4+0158); in other cases, the central galaxy is highly structured as in MS 1512.4+3647. The multiple-nuclei systems (e.g., MS 1244.2+7114 and MS 0440.5+0204) might be examples of cD galaxies under construction, as pointed out by Luppino et al. (1993) for MS 0440.5+0204, where the central galaxy may be cannibalizing smaller cluster members. Annis (1994) has pointed out an evolutionary effect in the morphologies of the brightest cluster members of the EMSS ($z = \frac{1}{3}$ sample) with respect to the $z = 0$ *HEAO 1* A-2 cluster sample (Piccinotti et al. 1982). The double morphologies are more often seen in the EMSS than in the present epoch ($z = 0$) *HEAO 1* brightest cluster galaxies; the triple systems seen in the EMSS are nonexistent in the *HEAO 1* sample. This fact could be taken as a preliminary evidence of morphological evolution in the brightest cluster galaxies at larger distances ($z \geq 0.3$).

As can be seen in the redshift histogram of Figure 3, the EMSS clusters constitute an excellent sample for cosmological studies. The average redshift for the full sample is $\langle z \rangle = 0.22$ with a dispersion $\sigma = 0.14$. The arc survey sample consists of the most luminous and distant of these clusters, and we note that all of the EMSS clusters with $z > 0.4$ meet the selection criteria for the arc survey sample. The redshift range encompassed by the clusters (possibly beyond z of 0.8) will allow the use of the sample for several projects to study the properties of clusters of galaxies at intermediate to large redshifts. Distant clusters provide important constraints on cosmological models. This same EMSS distant cluster sample provided evidence for the evolution of the X-ray luminosity function (Gioia et al. 1990b; Henry et al. 1992). The nature of the observed evolution (fewer high X-ray luminosity clusters in the past) is consistent with hierarchical structure formation. Henry et al. (1992) used the results to determine the shape and normalization of the mass fluctuation spectrum.

One of the motivations for the imaging survey was the search for gravitationally lensed arcs. We already mentioned the major improvement of an X-ray–selected sample compared to lens surveys based on optically selected clusters. In addition, the X-ray selection should have the property that the same kinds of objects are selected at differing redshifts. To draw inferences about clusters from a study of gravitational lensing, one has to understand whether the individual clusters are representative of the class as a whole. The X-ray selection assures the presence of a deep potential well and should therefore provide this representative sample. The fairly large number of lensed images that we are finding in this survey (Luppino et al. 1993, 1994; LeFèvre et al. 1994) gives us confidence that the EMSS cluster sample can be widely exploited for cosmological investigations.

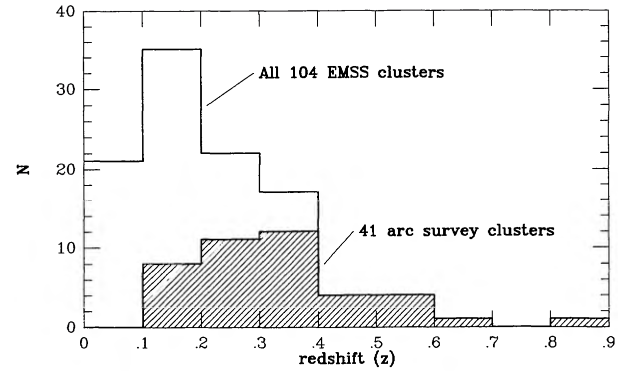

FIG. 3.—Redshift histogram for the entire EMSS cluster sample and for the 41 arc survey clusters. The mean redshift is $\langle z \rangle = 0.22$, and $\langle z \rangle = 0.32$ respectively.

We thank Jim Annis for assisting with some of the observing. This work was partially supported by NASA grants NAG5-1880, and NAG5-1752 and by NSF grant AST-9119216. The UH CCD cameras were fabricated with NSF grant AST-9020680. Radio data presented in this paper were obtained with the NRAO Very Large Array. The National Radio Astronomy Observatory (NRAO) is operated by Associated Universities, Inc., under contract with the National Science Foundation (NSF).

REFERENCES

Abell, G. O. 1958, ApJS, 3, 211
Abell, G. O., Corwin, H. G. & Olowin, R. P. 1989, ApJS, 70, 1
Annis, J. 1994, PhD thesis, Univ. of Hawaii
Bahcall, N. A. 1977, ApJ, 217, L77
———. 1980, ApJ, 238, L117
Couch, W., Ellis, R., Malin, D., & MacLaren, I. 1991, MNRAS, 249, 606
Donahue, M. E. 1990, PhD Thesis, Univ. of Colorado
Donahue, M. E., Stocke, J. T., & Gioia, I. M. 1992, ApJ, 385, 49
Dressler, A., & Gunn, J. 1992, ApJS, 78, 1
Edge, A. C., Stewart, G. C., & Fabian, A. C. 1992, MNRAS, 258, 177
Fabricant, D. G., Bautz, M. W. & McClintock, J. E. 1994, AJ, 107, 8
Fabricant, D. G., McClintock, J. E., & Bautz, M. W. 1991, ApJ, 381, 33
Fort, B., LeFèvre, O., Hammer, F., & Cailloux, M. 1992, ApJ, 399, L125
Frenk, C., White, S., Efstathiou, G., & Davis, M. 1990, ApJ, 351, 10
Garilli, B., Bottini, D., Maccagni, D., Vettolani, G., & Maccacaro, T. 1992, AJ, 104, 1290
Gioia, I. M., Geller, M. J., Huchra, J. P., Maccacaro, T., Steiner, J. E., & Stocke, J. T. 1982, ApJ, 255, L17
Gioia, I. M., Henry, J. P., Maccacaro, T., Morris, S. L., Stocke, J. T., & Wolter, A. 1990b, ApJ, 356, L35
Gioia, I. M., Maccacaro, T., Morris, S. L., Schild, R. E., Stocke, J. T. & Wolter, A. 1987, in Proc. 3d IAP Astrophysics Meeting, High Redshift and Primeval Galaxies, ed. J. Bergeron, D. Kunth, B. Rocca-Volmerange, & J. Tran Thanh Van (Paris: Editions Frontières), 231
Gioia, I. M., Maccacaro, T., Schild, R. E., Stocke, J. T., Liebert, J. W., Danziger, I. J., Kunth, D., & Lub, J. 1984, ApJ, 283, 495
Gioia, I. M., Maccacaro, T., Schild, R. E., Wolter, A., Stocke, J. T., Morris, S. L., & Henry, J. P. 1990a, ApJS, 72, 567
Gioia, I. M., et al. 1994, in preparation
Giraud, E. 1992, A&A, 259, L49
Gunn, J. E., Hoessel, G. J., & Oke, J. B. 1986, ApJ, 306, 30
Henry, J. P., Gioia, I. M., Maccacaro, T., Morris, S. L., Stocke, J. T., & Wolter, A. 1992, ApJ, 386, 408
Hoessel, J. G., Gunn, J., & Thuan, T. X. 1980, ApJ, 241, 486
Katgert, P., Thuan, T. X., & Windhorst, R. A. 1983, ApJ, 275, 1
Koo, D. C. 1981, ApJ, 251, L75
Kurtz, J. M., Huchra, J. P., Beers, T. C., Geller, M. J., Gioia, I. M., Maccacaro, T., Schild, R. E., & Stauffer, J. R. 1985, AJ, 90, 1665
Landolt, A. 1992, AJ, 104, 340
LeFèvre, O., Hammer, F., Angonin, M.-C., Gioia, I. M., & Luppino, G. A. 1994, ApJ, 422, L5
Luppino, G., Cooke, B., McHardy, I., & Ricker, G. 1991, AJ, 102, 1
Luppino, G. A., & Gioia, I. M. 1992, A&A, 265, L9
Luppino, G., Gioia, I., Annis, J., LeFèvre, O. & Hammer, F. 1993, ApJ, 416, 444
Luppino, G. A., et al. 1994, in preparation
Maccacaro, T., Gioia, I. M., Wolter, A., Zamorani, G., & Stocke, J. T. 1988, ApJ, 326, 680
Maia, M. A. G., da Costa L. N., Willmer, P. S., Pellegrini, P. S. & Rité, C. 1987, AJ, 93, 546
Mason, K. O., Spinrad, H., Bowyer, S., Reichert, G., & Stauffer, J. 1981, AJ, 86, 803

Mathez, G., Fort, B., Mellier, Y., Picat, J.-P., & Soucail, G. 1992, A&A, 256, 343
Mellier, Y., Fort, B., & Kneib, J.-P. 1993, ApJ, 407, 33
Nesci, R., Gioia, I. M., Maccacaro, T., Morris, S., Perola, G., Schild, R. E., & Wolter, A. 1989, ApJ, 344, 104
Nesci, R., Perola, G. C., & Wolter, A. 1994, A&A, submitted
Pesce, J. E., Fabian, A. C., Edge, A. C., & Johnstone, R. M. 1990, MNRAS, 244, 58
Piccinotti, G., Mushotzky, R. F., Boldt, E. A., Holt, S. S., Marshall, F. E., Serlemitsos, P. J., & Shafer, R. A. 1982, ApJ, 253, 485
Richter, O-G., & Huchtmeier, W. K. 1983, A&A, 125, 187
Soucail, G. 1992, in Clusters and Superclusters of Galaxies, ed. A. Fabian (NATO ASI Ser., 336) (Dordrecht: Kluwer), 199
Stark, A. A., Heiles, C., Bally, J., & Linke, R. 1984, Bell Labs, privately distributed magnetic tape
Stocke, J. T., Morris, S. L., Gioia, I. M., Maccacaro, T., Schild, R. E., Wolter, A., Fleming, T. A., & Henry, J. P. 1991, ApJS, 76, 813
White, S. D. M., Silk, J., & Henry, J. 1981, ApJ, 251, L65
Zamorani, G., Gioia, I. M., Maccacaro, T., & Wolter, A. 1988, A&A, 196, 39

Note added in proof.—After this paper was accepted for publication, we obtained multislit spectra with the CFHT for four clusters with previously uncertain redshifts. New redshifts and X-ray luminosities should be substituted in Table 1 for the following two clusters:

MS 1054.4−0321: $z = 0.8231 \pm 0.004$ (0 galaxies), $L_x = 9.281 \times 10^{44}$ *ergs* s^{-1};
MS 1137.5+6625: $z = 0.782 \pm 0.001$ (2 galaxies), $L_x = 7.559 \times 10^{44}$ *ergs* s^{-1}.

For MS 1610.4+6616, the value of $z = 0.55$ is still uncertain. The candidate MS 1209.0+3917 should be dropped from Table 1 since the redshifts obtained for five galaxies are not consistent with the identification of MS 1209.0+3917 as a cluster.